

1

FINAL TECHNICAL REPORT

FOR

AD-A215 343

DEPARTMENT OF THE NAVY
OFFICE OF NAVAL RESERACH

Grant No. N00014-89-J-1837

March 15, 1989 - March 14, 1990

DTIC
SELECTE
DEC 06 1989
S D^{cs} D

INTERNATIONAL CONFERENCE ON MATERIALS AND MECHANISMS OF
SUPERCONDUCTIVITY -- HIGH TEMPERATURE SUPERCONDUCTORS

By

Professor T.H. Geballe

Principal Investigator

Department of Applied Physics

Stanford University

Stanford, California 94305

DISTRIBUTION STATEMENT A
Approved for public release
Distribution Unlimited

October 1989



STANFORD UNIVERSITY
STANFORD, CALIFORNIA 94305-4090

DEPARTMENT OF APPLIED PHYSICS

Tel: (415) 723-0215
Fax: (415) 723-0010
E-Mail: Geballe@Sierra

November 28, 1989

Donald H. Liebenberg
Office of Naval Research
800 North Quincy Street
Arlington, Virginia 22217-5000

Dear Dr. Liebenberg:

Enclosed are three copies of the Final Technical Report for Grant No. N00014-89-J-1837, titled "International Conference on Materials and Mechanisms of Superconductivity - High Temperature Superconductors."

Sincerely,


T.H. Geballe, Professor
Department of Applied Physics

THG: png

Enclosures

Accession #		J
NTIS	SEARCH	
DTIC	TABLE	
Ungraded		
Justified		
By <i>per CS</i>		
Distribution		
Availability		
Dist	Availability	
A-1		

This work relates to Department of Navy Grant N00014-89-J-1837 issued by the Office of Naval Research. The United States Government has a royalty free license throughout the world in all copyrightable material contained herein.

MELTED FLUX LIQUIDS IN HIGH- T_c SUPERCONDUCTORS

David R. NELSON

Lyman Laboratory of Physics, Harvard University, Cambridge, Massachusetts 02138

A theory of the entangled flux liquids which arise in the new high- T_c superconductors is reviewed. New physics appears because of the weak interplanar couplings and high critical temperatures in these materials. Flux line wandering melts the conventional Abrikosov flux lattice over large portions of the phase diagram, and leads to a novel entangled vortex state. We suggest that a heavily entangled flux liquid could exhibit glassy behavior on experimental time scales, in analogy with viscoelastic behavior in dense polymer melts.

1. INTRODUCTION

One of the many fascinations of the CuO_2 -based superconductors⁽¹⁾ is the possibility of novel fluctuation effects due to the high critical temperatures and small coherence lengths. Although fluctuations are usually limited to the immediate vicinity of critical points, it was recently argued that fluctuations in the high- T_c materials lead to a new entangled flux liquid phase in a magnetic field, due to flux line wandering as vortex filaments traverse the sample.^{2,3}

These speculations are consistent with striking vibrating reed experiments by Gammel *et al.*,⁴ who find signal suggestive of flux lattice melting in single crystals of $\text{Bi}_2\text{Sr}_2\text{CaCu}_2\text{O}_8$ (BSCCO) at temperatures well below the onset of the Meissner effect.

Melted flux liquids are already familiar from discussions of two-dimensional superconducting films: Dislocation-mediated melting of the flux lattice leading to both ordinary and hexatic liquid phases of essentially point vortices was explored theoretically several years ago by D. S. Fisher.⁵ The novelty of high- T_c superconductors lies in the possibility of a melted liquid of entangled line defects in three dimensions.

We can estimate when the Abrikosov theory breaks down from a simple random walk argument.² We consider a single flux line $\vec{r}(z)$ and determine how far it wanders perpendicular to the z axis ($\vec{H} \parallel \hat{z}$) as it traverses the sample. In Ref. 3, it is shown that the vortex "diffuses" as a function of the time-like variable z ,

$$\sqrt{\langle |\vec{r}(z) - \vec{r}(0)|^2 \rangle} = \sqrt{2Dz} ,$$

where the "diffusion constant" D is given in terms of the mass anisotropy $M_{\perp}/M_{\parallel} \approx 10^{-2}$ and the vortex line tension ϵ_1 , by

$$D = \frac{M_{\perp}}{M_{\parallel}} \frac{k_B T}{\epsilon_1} .$$

At $T = 77$ K, we take $H_{c1} \approx 10^3$ G (which determines ϵ_1) and $M_{\parallel}/M_{\perp} \approx 10^2$ and find $D = 10^{-6}$ cm, so that vortex lines wander a distance of order 1 micron while traversing a sample of thickness 0.01 cm. This diffusive behavior implies an entanglement correlation length,^{2,3} $\xi_z \approx 1/2Dn$, which is the distance required to wander a vortex spacing in a vortex liquid with areal density $n = B/\phi_0$. Collisions and entanglement of vortex lines will significantly alter the Abrikosov theory whenever

$$L \gg \xi_z ,$$

where L is the sample thickness.

2. LINDEMANN CRITERION AND PHASE DIAGRAM

To determine where the flux lattice melts, we assume that the external field is aligned with the z -direction, perpendicular to the CuO_2 planes, and describe the trajectory of the i -th vortex by a function $\vec{r}_i(z)$. If the average position of the i -th vortex in a

triangular lattice denoted by \vec{R}_i , we can define a two-dimensional displacement field $\vec{u}(\vec{R}_i, z)$ by

$$\vec{r}_i(z) = \vec{R}_i + \vec{u}(\vec{R}_i, z)$$

In the continuum limit, this displacement becomes a function $\vec{u} = \vec{u}(x, y, z)$. The excess free energy $\delta\bar{G}\{\vec{u}(\vec{r})\}$ associated with small gradients of \vec{u} is⁶

$$\delta G\{\vec{u}(\vec{r})\} = \frac{1}{2} \int d^3r \left[2\mu u_{\alpha\beta}^2 + \lambda u_{\delta\delta}^2 + K \left(\frac{\partial \vec{u}}{\partial z} \right)^2 \right]$$

where

$$u_{\alpha\beta}(\vec{r}) = \frac{1}{2} \left(\frac{\partial u_\alpha}{\partial r_\beta} + \frac{\partial u_\beta}{\partial r_\alpha} \right), \quad \alpha, \beta = x, y$$

is the symmetrized two-dimensional strain matrix, μ and λ are Lamé coefficients, and K is a tilt elastic constant. The mean-square displacement of a vortex is then (assuming $2\mu + \lambda \gg \mu$)

$$\langle |\vec{u}(\vec{r}_0)|^2 \rangle \approx \sqrt{\frac{n}{4\pi}} \frac{k_B T}{\sqrt{\mu K}}$$

According to the Lindemann criterion, melting will occur when $\sqrt{\langle u^2 \rangle}$ exceeds, say, $\frac{1}{10}$ of the lattice constant. To evaluate Eq. (3), we need estimates of μ and K .

Although the shear modulus will be of order its value in isotropic superconductors,⁷ the tilt modulus K will typically be much smaller than the isotropic value⁸ $K = \frac{HB}{4\pi}$ when the anisotropy of high- T_c materials is taken into account. A reasonable guess, valid for $H_{c1} \ll H \ll H_{c2}$, is³

$$K \approx \frac{M_\perp}{M_\parallel} \frac{HB}{4\pi}, \quad (1)$$

where M_\perp is the in-plane effective mass, and $M_\parallel \approx 10^2 M_\perp$ is the much larger mass describing the weak coupling between CuO_2 planes. The tilt modulus is small because the magnetic field does not rotate appreciably when vortex lines are tilted in a highly anisotropic superconductor.⁸

The field remains essentially uniform and perpendicular to the CuO_2 planes whenever $d \ll \lambda$, where d is the vortex spacing and λ is the London penetration depth. The estimate (4) breaks down near H_{c2} because most of the material is in its normal state, and the macroscopic magnetic properties must then reflect the (small) magnetic anisotropy of a normal metal. As pointed out by D. Huse,⁹ Eq. (1) also breaks down near H_{c1} , because of the magnetic dipole coupling between vortices present for $d \geq \lambda$. Over the large range of fields where (1) is valid, it is easy to estimate the root mean square phonon displacements and show that the BSSCO flux lattice is indeed melted over a wide range of fields and temperatures.³

The Lindemann criterion assumes wave vector-independent elastic constants which can be a gross oversimplification, especially if fluctuations are important. A more accurate theory would use wave vector dependent elastic constants.³ This has been done by Houghton, Pelcovits, and Sudbo,¹⁰ who generalize nonlocal elastic constants derived by Brandt.⁷ As pointed out by Houghton *et al.*, there are significant corrections to the Lindemann criterion due to nonlocal effects in high- T_c materials. These nonlocal effects act to enhance the fluctuation induced melting considered above. By using the Lindemann ratio as a fitting parameter [they find $\sqrt{\langle u^2 \rangle} = 0.4d$ at melting], these authors are able to obtain good fits to the melting curves of Ref. 6 for both YBCO and BSCCO.

The Lindemann analysis sketched above cannot be correct in the vicinity of H_{c1} , i.e., when the flux line spacing is of order the London penetration depth or more. This is the regime of most flux decoration experiments. The classical theory, based on energetic considerations alone, predicts that $\mu \sim \lambda \sim \exp(-d/\lambda)$ as the vortex separation $d \rightarrow \infty$.⁷ There are, however, important entropic effects due to flux line wandering which dominate over flux line interaction energies in the dilute

limit. It can be shown that the effect of these fluctuations is to produce a thin sliver of melted flux liquid phase just above H_{c1} .^{3,11,12}

Figure 1 shows a schematic phase diagram for BSCCO which combines the high field Lindemann criterion melting curves of Houghton *et al.*¹⁰ with the low field estimate of the melting curve discussed

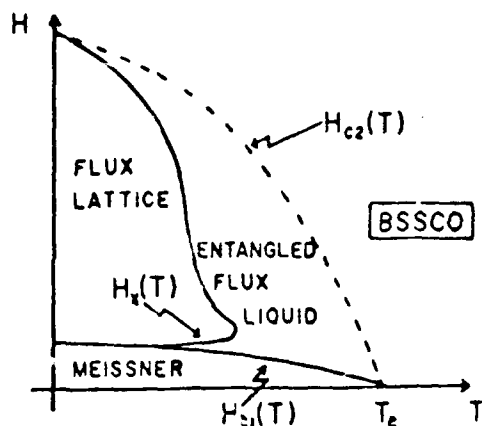


Fig. 1. Schematic phase diagram for BSCCO with \vec{H} directed perpendicular to the CuO_2 planes.

above.^{11,12} The field is assumed to be perpendicular to the CuO_2 planes. The region occupied by the entangled flux liquid is smaller for YBCO than for BSCCO, because M_x/M_L is much smaller in this case. For most conventional superconductors, the reentrant melting curve $H_z(T)$ is indistinguishably close to $H_{c1}(T)$ and $H_{c2}(T)$. The mean-field transition line at H_{c2} need not be a sharp phase transition when fluctuations are taken into account;^{12,13} experimentally it is defined by the onset of an (incomplete) Meissner effect with decreasing temperatures.

3. PROPERTIES OF THE ENTANGLED FLUX LIQUID

The entangled flux liquid is a new phase of matter,

stabilized by the entropy available when flux lines entangle. Of particular interest is the vortex line correlation function, which can be measured with neutron scattering.¹⁴ These experiments measure fluctuations in the local density of flux lines, defined by

$$n(\vec{r}_\perp, z) = \sum_{i=1}^N \delta[\vec{r}_\perp - \vec{r}_i(z)] .$$

Neutron scattering measures

$$\hat{S}(\vec{q}_\perp, q_z) = \langle |n(\vec{q}_\perp, q_z)|^2 \rangle ,$$

where $n(\vec{q}_\perp, q_z)$ is the Fourier transform of $n(\vec{r}_\perp, z)$. The physics, however, is more conveniently discussed in terms of the partial Fourier transform

$$\begin{aligned} S(\vec{q}_\perp, z) &= \int_{-\infty}^{\infty} \frac{dq_z}{2\pi} e^{-iq_z z} \hat{S}(\vec{q}_\perp, q_z) \\ &= \langle n(\vec{q}_\perp, z + z_0) n_\perp^*(\vec{q}_\perp, z_0) \rangle . \end{aligned} \quad (2)$$

This correlation function reduces to the structure function of a cross-section of the vortex lines when $z = 0$. The correlations in any such constant z cross-section should be similar to those of a two-dimensional liquid. Equation (2) describes more generally how the Fourier components of this 2d structure function decay along the z -axis due to entanglement. As shown in Ref. 3 (by exploiting an analogy with superfluidity in two-dimensional bosons) this decay can be approximated by

$$S(\vec{q}_\perp, z) \approx S(\vec{q}_\perp, z=0) e^{-\epsilon(q_\perp) |z| / k_B T} , \quad (3)$$

where $\epsilon(q_\perp)$ is the phonon-roton excitation spectrum of the corresponding superfluid. The excitation spectrum defines via Eq. (3) a q_\perp -dependent correlation length

$$\xi_{\parallel}(q_\perp) \equiv k_B T / \epsilon(q_\perp) .$$

The quantity $\xi_{\parallel}(q_\perp)$ equals the "entanglement correlation length" ξ_s when $q_\perp \sim 1/d$, where d is an

intervortex spacing.³

There is also interesting modifications of the $B(H)$ constitutive relation near H_{c1} where the transition from the Meissner phase is into an entangled flux liquid.^{2,3} A discussion of the hydrodynamics of equilibrated flux liquids is in preparation.¹⁵

4. SLUGGISH DYNAMICS DUE TO ENTANGLEMENT

Disorder will be most effective in suppressing flux flow resistivity in vortex phases which exhibit a nonzero shear modulus on experimental time scales. In conventional superconductors, for example, a few securely pinned flux lines can pin the entire flux lattice if there is large shear rigidity. We argue here that very long shear relaxation times may also be possible in an entangled flux liquid.³ Although it will greatly affect the response to a dilute concentration of pinning centers, this mechanism for obtaining a shear modulus does not require pinning centers to work.

Figure 2 shows a heavily entangled flux liquid, view-

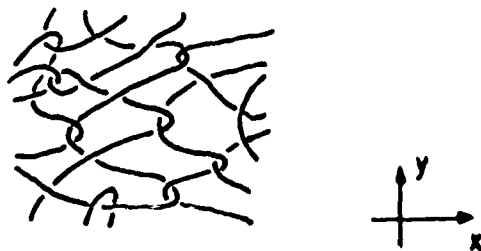


Fig. 2. Schematic top view of an entangled flux liquid. Each flux line executes a two-

dimensional random walk, occasionally entwining around one of its near neighbors. Figure 2 is like a two-dimensional polymer melt, with the understanding that polymers which appear to cross in the projection are actually ordered, one above the other, according to which of the crossing lines has the largest z coordinate. The z coordinate plays the role of a monomer index in this polymer analogy.

If the configuration of vortex lines in Figure 2 is subjected to a shear stress σ_{xy} , the constraints provided by the entanglements in this figure will make relaxation difficult. The notion of constraints requires a large barrier to flux line cutting. When two lines, both approximately parallel to \vec{H} , cross, they must pass over a barrier of order $2\epsilon_1 l$, where ϵ_1 is the line tension, and l is the distance along \vec{H} over which the crossing occurs. This barrier arises because, as two lines cross, they behave like single double quantized vortex over the distance l . The supercurrents responsible for this barrier flow primarily within the CuO_2 planes, due to the anisotropy.⁸ Upon expressing ϵ_1 in terms of the lower critical field, we find

$$\frac{2\epsilon_1 l}{k_B T} = \frac{H_{c1} \phi_0 l}{2\pi k_B T} \approx 50, \quad (4)$$

where we have set $H_{c1} = 80$ Oe, $l = 10 \text{ \AA}$, and $T = 77$ K. Thus, line crossings will be very difficult, just as for polymers in an entangled melt.

The analogy with polymer melts¹⁶ suggest that, after an initial transient, the strain u_{xy} will be proportional to the applied stress for times $t < \tau_L$,

$$u_{xy} \approx \sigma_{xy} / \mu_0,$$

which defines a shear modulus μ_0 for times shorter than the relaxation time τ_L . For times longer than τ_L , the material will behave like a viscous liquid, with the strain rising linearly with t ,

$$u_{xy} \approx \sigma_{xy} t / \eta,$$

which defines a shear viscosity η . The key quantity in this description of the viscoelastic response is the relaxation time τ_L , which, for polymers, is a strong function of the polymerization index.

The analogous time scale in entangled flux liquids will be a sensitive function of the sample thickness L . To estimate this time, we use the de Gennes reptation theory of polymeric relaxation in three dimensions,¹⁶ in which each polymer is assumed to diffuse along a "tube" defined by the entanglement constraints. A very similar situation arises in the two-dimensional polymeric problem considered here. The de Gennes theory predicts that τ_L varies approximately as the cube of the sample thickness

$$\tau_L = \tau_0(L/\xi'_s)^3,$$

where τ_0 is a microscopic time, and we expect that ξ'_s is of the order of the entanglement correlation length. Motion of the center of mass of a single vortex line is described by the diffusion constant¹⁶

$$D_L = D_0(L/\xi'_s)^{-2},$$

where D_0 is the diffusion constant of a point vortex in, say, an isolated CuO_2 plane. A rough estimate is $D_0 \sim \hbar/m_s \sim 1 \text{ cm}^2/\text{sec}$. The microscopic relaxation time should be of order

$$\tau_0 \sim 1/D_0 n \sim \phi_0/D_0 B.$$

If the intervortex spacing is $d = (\phi_0/B)^{1/2} \approx 100 \text{ \AA}$ and $\xi'_s = 2000 \text{ \AA}$, we find from Eq. (13) that $\tau_L = 10^3 \text{ sec}$ or about 15 min for $L = 1 \text{ cm}$. The shear viscosity in this regime should be of order¹⁶

$$\eta \approx \tau_L \mu_0,$$

or $\eta \approx 2 \times 10^4$ poise using standard estimates⁷ of μ_0 with $H = \frac{1}{2} H_{c2}$.

The ideas sketched above suggest that regimes of very high viscosity (over 10^6 times that of water) are

possible in sufficiently thick samples. Because the line tension ϵ_1 vanishes near H_{c2} , one must be sufficiently far below the mean field $H_{c2}(T)$ before the barrier (4) associated with entanglement becomes effective. One might even speculate that the sluggish dynamics which results with decreasing temperature is the origin of the "irreversibility lines" like those discussed by Malozemoff *et al.*¹⁷

ACKNOWLEDGEMENTS

It is a pleasure to acknowledge the collaboration of H. Sebastian Seung which led to Ref. 5. This work was supported by the National Science Foundation through grant DMR-8817291 and through the Harvard Materials Research Laboratory.

REFERENCES

1. M. Rice, Z. Phys. 67B (1987) 141 and references therein.
2. D. R. Nelson, Phys. Rev. Lett. 60 (1988) 1973.
3. D. R. Nelson and H. S. Seung, Phys. Rev. B39 (1989) 9153.
4. P. L. Gammel, L. F. Schneemeyer, J. V. Waszczak, and D. J. Bishop, Phys. Rev. Lett. 61 (1988) 1666.
5. D. S. Fisher, Phys. Rev. B22 (1980) 1190.
6. P. G. deGennes and J. Matricon, Mod. Phys. 36 (1964) 45.
7. E. H. Brandt and U. Essman, Phys. Stat. Sol. 144 (1987) 13, and references therein.
8. V. G. Kogan, Phys. Rev. B24 (1981) 1572.
9. D. Huse, private communication. A similar electromagnetic coupling is responsible for the DC transformer effect. See, e.g., J. W. Ekin, B. Serin, and J. R. Chen, Phys. Rev. B9 (1974) 912.
10. A. Houghton, R. A. Pelcovits, and A. Sudbo, Phys. Rev. B, in press.
11. D. R. Nelson, J. Stat. Phys., in press.
12. Phase diagrams similar to those in Fig. 1 have also been constructed by D. S. Fisher, M. P. A. Fisher, and D. Huse, manuscript in preparation.

13. M. P. A. Fisher and D. H. Lee, Phys. Rev. B38 (1989) 2756.
14. D. Cribier, B. Jacrot, L. M. Rao, and B. Farnoux, Phys. Rev. Lett. 9 (1964) 106.
15. M. C. Marchetti and D. R. Nelson, to be published.
16. P. G. de Gennes, Scaling Concepts in Polymer Physics (Cornell Univ. Press, Ithaca, 1979).
17. A. P. Malozemoff, T. K. Worthington, Y. Yeshurun, and F. Holtzberg, Phys. Rev. B36 (1988) 203, and references therein.

ANISOTROPY IN MAGNETIC PROPERTIES OF HIGH-T_c MATERIALS

Vladimir G. KOGAN

Iowa State University, Ames Laboratory and Physics Department, Ames, IA 50011 (currently at Theoretical Physics Institute, University of Minnesota, 116 Church St.S.E., Minneapolis, MN 55455)

A brief review is given on recent results concerning equilibrium flux-line lattices, the field distribution within a cell of vortex lattices, the transverse magnetization and the anisotropy related torque. Current carrying properties of boundaries between misaligned anisotropic superconductors are discussed.

This brief review is intended to summarize the recent results and to provide a reference, however selective and incomplete, for anyone entering the rapidly expanding subject of the title. The simple way to describe *major* anisotropy effects is to replace in the London or Ginzburg-Landau equations the squares of the isotropic penetration depth and of the coherence length, λ^2 and ξ^2 , with tensors $(\lambda^2)_{ik} = \lambda^2 m_{ik}$ and $(\xi^2)_{ik} = \xi^2 m_{ik}^{-1}$, respectively. Tensor m_{ik} (usually called "mass-tensor", although it is related to the superfluid density and incorporates all sources of anisotropy of the tensor type) is normalized on the average mass $(M_1 M_2 M_3)^{1/3}$, where M 's are the principal values of M_{ik} . The average values, λ and ξ , are related to the principal values: $\lambda^3 = \lambda_1 \lambda_2 \lambda_3$, $\xi^3 = \xi_1 \xi_2 \xi_3$. Note, that only the "squares", $(\lambda^2)_{ik}$ and $(\xi^2)_{ik}$, transform as tensors under coordinate transformations. Also, not all anisotropy effects can be described with this simple approach; e.g., a possible anisotropy in the basal plane of tetragonal materials is completely missed in this description. Still, in materials of interest the basal plane anisotropy is usually weak, and m_{ik} approach provides a simple and unified description of various effects of the strong

"c-a" anisotropy.

The only restriction for the London theory to hold is a *spacially constant* modulus of the order parameter. This is fulfilled in fields $H \ll H_{c2}$, where the vortex cores of the size ξ are not overlapped, the usual situation for high-T_c materials. The *absence of any restriction upon T* and the simplicity make the London approach a useful tool in studying magnetic properties of high-T_c's. We will concentrate in the following on results obtained within this approach.

Using the London free energy^{1,2}

$$F = \int (h^2 + \lambda^2 m_{ik} \text{curl}_i h \text{curl}_k h) dv / 8\pi, \quad (1)$$

one can compare different flux arrangements and find one corresponding to the thermodynamic equilibrium. For intermediate applied fields H_a , $H_{c1} \ll H_a \ll H_{c2}$, this was done in Ref. 3 for the uniaxial case. The magnetization M in this domain is on the order of H_{c1} and therefore is small with respect to B , H and H_a ; the three latter vectors are almost the same in value and direction. This simplifies the problem allowing to disregard demagnetization effects. For the field at an angle θ to the c direction of the crystal the flux line lattice (FLL) in the plane normal to B is made of isosceles triangles with the base-to-side

ratio of $\sqrt{1+3m_c/m_a}/2$, where $m(\theta) = m_a \sin^2\theta + m_c \cos^2\theta$. The short base is directed along the projection of c onto the plane normal to B ; the long height of the triangle is situated in the ab plane. The FLL is locked upon the crystal; any rotation of the FLL as a whole round B causes an energy increase, the feature absent in isotropic materials. The same equilibrium FLL has been found near H_{c1} ,² near H_{c2} ,⁴ and as a particular case in a more general context of 3 different masses.⁵ Decoration experiments for $B \perp c$ on Y-123 are consistent with London predictions.⁶

Given the equilibrium FLL, one can study the field $h(r)$ within an FLL cell. This is done by solving the London eqs in the Fourier space and then by the numerical reconstruction of $h(r)$.^{7,8} Three relevant results are to be mentioned:

(a) For an arbitrary orientation of vortex axes (of B) within a crystal, the local $h(r)$ has a non-zero component, $h_{tr}(r)$, transverse to B . Thus, h is not parallel to B , unless B points in one of the principal directions. Physically, h_{tr} is related to the tendency of persistent currents to flow along directions with small masses which would reduce the kinetic contribution to the free energy (the second term in Eq.(1)).

(b) The transverse field compares in value to the familiar longitudinal field $h_{lg} = h \cdot B/B$, provided the average vortex separation exceeds λ (near H_{c1}).¹ In fields well above H_{c1} , h_{tr} is on the order H_{c1} , i.e. it is small with respect to B .^{2,8} However, in any field, h_{tr} scales with the variable part of h_{lg} . Roughly, h_{tr} scales with the macroscopic magnetization M ; h_{tr} cannot be neglected as long as properties related to the field variation (such as M) are concerned.

(c) The average $\langle h_{tr} \rangle$ over the FLL cell is zero. This manifestation of the flux quantization has been established in Ref. 9 for H close to H_{c2} . The argument used holds in any field. Numerical results of Ref. 8 comply well with this restriction.

Due to the "extra" energy dependence upon rotations, the elastic properties of FLL's in anisotropic superconductors are richer than in the isotropic case. Second order terms of the energy expansion in derivatives of the displacement u , contain not only terms quadratic in strains $u_{ik} =$

$(\partial u_i / \partial x_k + \partial u_k / \partial x_i) / 2$, but also those quadratic in rotations $\omega_{ik} = (\partial u_i / \partial x_k - \partial u_k / \partial x_i) / 2$, as well as ones proportional to $u_{ik} \omega_{ik}$. The 2D elastic constants for the FLL deformations that conserve the direction of vortex axes, has been considered in Ref. 10. A

potentially relevant conclusion: the anisotropy influence upon the elastic properties of FLL's is much stronger than upon such common features of interest as H_{c2} , H_{c1} or M . It turned out, e.g., that in 2D there exist two independent shear modulae, $C_{66,hard}$ and $C_{66,easy}$ whose ratio is $(m_c/m_a)^2$ (which amounts to $(m_c/m_a)^2$ for $B \perp c$). Recall that the ratio of H_{c2} 's in two principal directions is only $(m_c/m_a)^{1/2}$. The hard shear mode corresponds to displacements along the base of the elementary triangle, whereas the easy one describes the shear deformation, in which displacements are in the ab plane (along the long dimension of the triangle). For the field in the ab plane even the "moderately" anisotropic Y-123, $(m_c/m_a)^{1/2} = 5$, the ratio of the two shear modulae exceeds 600. In the Bi-2212 the estimates of the $(m_c/m_a)^{1/2}$ range from 17 (Ref.16) to more than 50 (Ref.19), putting the ratio of shears

between 10^5 and 10^7 . The FLL, therefore, is very stiff with respect to the hard shear mode and is very soft with respect to the easy one (in which vortices slide along the ab plane). The decoration results of Dolan *et al*⁶ for $B \perp c$ are consistent with the lattice being very soft with respect to "sliding" deformations. On the other hand, Biggs *et al*¹¹ concluded that there is no observable creep of vortices ($B \perp c$) along c in Bi-2212 crystals. This is expected if the corresponding shear modulus ($C_{66,hard}$ in this case) is large. The failure of the FLL (again for $B \perp c$) to show a detectable response to the Lorentz force along c in experiments with oriented films of Bi-2212 (Ref.12) and of Tl-2212 (Ref.13) may also be interpreted as an indication of a large $C_{66,hard}$ (in a Y-123 single crystal this response is found to be finite but weak, Ref.14).

One of the macroscopic effects of the non-zero transverse field in vortices of anisotropic materials is the transverse (to B) component of the magnetization M_{tr} . One can evaluate M if the free energy of the FLL is known as a function of B .^{3,15} The M_{tr} can be measured directly¹⁶ or by observing the torque $\tau = |M \times B| = M_{tr}B$. In intermediate fields the torque data¹⁷ for Y-123 are in a good agreement with the London theory.¹⁸ The data should be taken at sufficiently high temperatures and fields, where M is reversible to assure that the torque measured is an intrinsic anisotropy-related property (as opposed to torques due to a trapped flux or due to the shape effects). The low- J_c material Bi-2212 provides a broad window in the T-H plane where such measurements can be done; the ratio $(m_c/m_a)^{1/2}$ extracted from the torque data exceeds 50.¹⁹

It should be pointed out that among various methods of extracting the anisotropy

parameter $\gamma = \sqrt{m_c/m_a}$, the H_{c1} measurements show consistently lower values than those obtained by other means. For Y-123 estimates of H_{c1} produce $\gamma=3$,²⁰ while magnetization,²¹ torque,¹⁷ H_{c2} , and decoration⁶ yield $\gamma=5$ or more. The discrepancy is pronounced in the case of Bi-2212, for which the H_{c1} data suggest again $\gamma=3$,^{22,23} whereas the torque technique generates $\gamma=55$,¹⁹ and the H_{c2} gives about 60.²⁴ The subject of the H_{c1} anisotropy deserves further study. At this stage, one may speculate that the maximum H_{c1} for $H \parallel c$ might be underestimated if the crystal has planar defects parallel to c , which allow the vortices to penetrate the sample at $H < H_{c1}$. The minimum H_{c1} for $H \perp c$, on the other hand, can be over-estimated due to the platelet-like crystal shapes and possible surface barriers in fields parallel to platelet faces. A small misalignment between the applied field and the ab -plane may again result in an overestimate of the " H_{c1} parallel to ab ". While it is conceivable that the first of the reasons given, is responsible for an under-estimate of $H_{c1,max}/H_{c1,min}$ for Y-123, it is not yet clear whether the last two are sufficient for resolving the discrepancy for the Bi-compound.

In order to address problems of the current flow in polycrystalline samples within the London approach, one has to formulate the conditions at the boundaries between misaligned anisotropic superconductors.²⁵ Perhaps, the simplest way to obtain these conditions has been suggested by N.Schopohl: integrate the London eqs., $h + \lambda^2 \text{curl} \mathbf{I} = 0$, where the vector $\mathbf{I}_k = (4\pi/c)m_{kn}j_n$, over the area of a contour which crosses the interface. When the contour shrinks in a direction normal to the

boundary so that its long sides run along the interface in the opposite directions, the integral of \mathbf{h} vanishes. Thus, $\int \text{curl } \mathbf{I} \cdot d\mathbf{s} = \oint \mathbf{I} \cdot d\mathbf{l} = 0$, i.e. the tangential components of \mathbf{I} must be the same on both sides of the interface: $(m_{tn}j_n)_{\text{left}} = (m_{tn}j_n)_{\text{right}}$, where t denotes any of the tangential directions. This peculiar condition means that for a general misalignment where m_{ik} on both sides may have non-zero off-diagonal components, *the tangential and normal components of j at the interface are coupled*. In general, *any transport current through the boundary must be accompanied by a current along the boundary*. The latter flows in opposite directions at opposite sides of the interface and creates an "extra" magnetic field parallel to the interface, that decays with the distance from the boundary. As a result, boundaries between anisotropic superconductors may serve as channels, along which vortices can penetrate the sample at a field smaller than the H_{c1} 's of both crystals in contact. The total current undergoes a "refraction" at the boundary. In short, boundaries distort the current flow and the distortion extends on distances of the order λ on both sides. Another possibility is discussed in Ref.25: the spontaneous creation of vortex chains at sufficiently long boundaries may lead to an extra dissipation whenever the persistent current crosses the interface.

Some support for the presentation of this work relates to Department of Navy Grant N00014-89-J-1837 issued by the Office of Naval Research. The US Government has a royalty-free license throughout the world in all copyrightable material contained herein.

1. V.G.Kogan, Phys. Rev. B, 24, 1572 (1981).
2. A.V.Balatskii et al, Sov. Phys. JETP 63, 866 (1986).
3. L.J.Campbell et al, Phys. Rev. B 38, 2439 (1988).
4. K.G.Petzinger, to be published.
5. N.Schopohl and A.Baratoff, to be published.
6. G.J.Dolan et al, Phys.Rev.Lett, 67, 2184 (1989).
7. N.Schopohl and A.Baratoff, Physica C 153-155, 689 (1988).
8. S.Thiemann et al, Phys.Rev. 39 11406 (1989).
9. V.G.Kogan and J.R.Clem, Phys. Rev. B 24, 2497 (1981).
10. V.G.Kogan and L.J.Campbell, Phys. Rev. Lett. 62, 1552 (1989).
11. B.D.Biggs et al, Phys. Rev. B 39, 7309 (1989).
12. Y.Iye et al, Report of ISSP, University of Tokyo, Ser. A, No 2138, May 1989.
13. K.C.Woo et al, subm. to Phys. Rev. Lett.
14. G.W.Crabtree, privat communication.
15. V.G. Kogan et al, Phys. Rev. B 38, 11958 (1989).
16. M.Tuominen, private communication.
17. D.E.Farrell et al, Phys.Rev.Lett. 61, 2805 (1988).
18. V.G.Kogan, Phys. Rev.B 38, 7049 (1988)
19. D.E.Farrell et al, subm. to Phys.Rev.Lett.
20. L.Krusin-Elbaum et al, Phys.Rev.B 39, 2936 (1989).
21. S.Mitra et al, to be published in Phys.Rev.B.
22. L.Krusin-Elbaum et al, to be published.
23. M.Wacenovsky et al, preprint.
24. T.Palstra et al, Phys.Rev.B 38, 5102 (1988).
25. V.G.Kogan, Phys.Rev Lett. 62, 3001 (1989).

PHENOMENOLOGICAL THEORY OF MAGNETIC STRUCTURE IN THE HIGH-TEMPERATURE SUPERCONDUCTORS

John R. CLEM

Ames Laboratory-USDOE and Department of Physics, Iowa State University, Ames, Iowa 50011, U.S.A.*

In the absence of a complete microscopic theory of the high-temperature copper-oxide superconductors, several phenomenological theoretical approaches are being used to describe the intragranular magnetic structure in the mixed state. The purpose of this paper is to review these approaches and to point out where further developments are needed.

1. INTRODUCTION

Since the discovery of the high-temperature oxide superconductors,¹ these materials have been known to have magnetic properties characteristic of type-II superconductors. Although the properties of bulk sintered samples of these materials are greatly complicated by the effects of granularity,² we ignore such effects in this paper and focus on how to theoretically describe the intragranular magnetic structure in ideal untwinned single crystals, which are known to be highly anisotropic. We first discuss two main approaches. One is to treat the magnetic structure within either the London theory³⁻⁴ or the Ginzburg-Landau theory⁵⁻¹⁶ with an anisotropic effective mass tensor, and the other is to model a layered superconductor as a stack of Josephson-coupled superconducting blocks or layers.¹⁷⁻²⁰ We then describe the connections between these two approaches and briefly discuss desired extensions of the theory.

2. ANISOTROPIC EFFECTIVE-MASS THEORY

The simplest way to account for anisotropy effects in the mixed state of the high-temperature superconductors is to express the anisotropy in terms of a phe-

nomological effective-mass tensor in the framework of the London³⁻⁴ or Ginzburg-Landau⁵⁻¹⁶ theories, which normally are taken to be isotropic. In the reference frame aligned with the principal axes, this mass tensor is diagonal, and the diagonal elements m_i ($i = 1, 2, 3 = a, b, c$) are normalized¹³⁻¹⁴ such that $m_1 m_2 m_3 = 1$. The penetration depths $\lambda_i = \lambda \sqrt{m_i}$ describe the decay of components of the supercurrent along the principal directions, and the corresponding coherence lengths $\xi_i = \xi / \sqrt{m_i}$ characterize the spatial variation of the order parameter along these directions. The scalars $\lambda = (\lambda_1 \lambda_2 \lambda_3)^{1/3}$ and $\xi = (\xi_1 \xi_2 \xi_3)^{1/3}$ enter the Ginzburg-Landau expressions for the bulk thermodynamic critical field $H_c = \phi_0 (\sqrt{2}) 2\pi \lambda \xi$ (a scalar) and the Ginzburg-Landau parameter $\kappa = \lambda \xi$.

Recent vortex-lattice decoration experiments²¹⁻²² have shown that in $\text{YBa}_2\text{Cu}_3\text{O}_{7-\delta}$ the penetration depths are approximately in the ratios $\lambda_a : \lambda_b : \lambda_c = 1.2 : 1 : 5.5$. These results thus give $m_a = 0.4$, $m_b = 0.3$, and $m_c = 8.8$. To explain these results qualitatively, we can say that the penetration depths λ_a and λ_b are much smaller than λ_c because the screening currents along the CuO_2 planes (in the a or b direction) flow much more easily than in the c direction. Moreover,

*Ames Laboratory is operated for the U.S. Department of Energy by Iowa State University under Contract No. W-7405-Eng-82. This work was supported by the Director for Energy Research, Office of Basic Energy Sciences. Some support for the presentation of this work relates to Department of Navy Grant N00014-89-J-1837 issued by the Office of Naval Research. The United States Government has a royalty-free license throughout the world in all copyrightable material contained herein.

λ_b in $\text{YBa}_2\text{Cu}_3\text{O}_{7-\delta}$ is somewhat smaller than λ_a because current parallel to the CuO_2 planes flows more easily along the CuO chains (in the b direction) than perpendicular to these chains (in the a direction).

It is important to realize that the penetration depth depends upon the direction of the screening supercurrent density \mathbf{j} , not upon the direction of the local magnetic field \mathbf{b} .^{4,13,16} Suppose, for example, an untwinned single crystal is cleaved normal to a principal axis, so as to expose a flat surface in the yz -plane. Application of a weak applied magnetic field H_a along a principal axis parallel to the surface generates a screening current density \mathbf{j} along the other principal axis that is parallel to the surface. This component of \mathbf{j} and its corresponding local magnetic field \mathbf{b} [$(4\pi/c)\mathbf{j} = \nabla \times \mathbf{b}$] decay exponentially as $\exp(-x/\lambda_i)$, where x is the distance into the sample and the subscript i refers to the axis along which \mathbf{j} flows.

Within Ginzburg-Landau theory with an anisotropic mass tensor,⁵⁻¹⁶ the magnetic field penetration is governed by Maxwell's equations plus the second Ginzburg-Landau equation,

$$j_i = -(c^2/4\pi\lambda_i^2)a_{si}. \quad (1)$$

This equation gives the connection between the i th ($i = 1, 2, 3 = x, y, z$) component of the supercurrent density \mathbf{j} and the i th component of the gauge-invariant vector potential $\mathbf{a}_s = \mathbf{a} + (\phi_0/2\pi)\nabla\gamma$. Here, \mathbf{a} is the vector potential ($\mathbf{b} = \nabla \times \mathbf{a}$) and γ is the phase of the reduced order parameter $f \exp(i\gamma)$, which can be regarded as the Cooper-pair wave function.

For a vortex centered on the x -axis (a -axis), the London-model^{13,23} expression for the magnetic field, derived assuming $f = 1$ outside the core, is

$$b_x(y, z) = (\phi_0/2\pi\lambda_b\lambda_c)K_0\{[(y/\lambda_c)^2 + (z/\lambda_b)^2]^{1/2}\}, \quad (2)$$

where K_0 is the modified Bessel function of order zero. The decay with distance along the y -axis (b -axis) is approximately exponential, with decay length λ_c . The reason that the decay length is λ_c and not λ_b is that the decay length is associated with the direction of the screening currents, and on the y -axis these

currents point in the z direction. Similarly, along the z -axis (c -axis) the screening currents flow parallel to the b direction and hence the magnetic field decays exponentially with decay length λ_b . Contours of constant b_x and streamlines of \mathbf{j} are ellipses: $(y/\lambda_c)^2 + (z/\lambda_b)^2 = \text{const}$.

The core of the London-model vortex is defined by the ellipse $(y/\lambda_c)^2 + (z/\lambda_b)^2 = (\xi_b/\lambda_c)^2 = (\xi_c/\lambda_b)^2 = m_a^2/\kappa^2 = 1/\kappa_a^2$. Here $\kappa = \lambda/\xi$ is the Ginzburg-Landau parameter and $\kappa_a = \kappa/\sqrt{m_a}$ is an effective κ for a vortex aligned along the a direction. The semi-major axis along the y -axis (b -axis) is ξ_b , and the semi-minor axis along the z -axis (c -axis) is ξ_c . Inside the core, $b_x = \text{const}$ and $f = 0$ according to the London model. Calculation of the energy per unit length of the vortex along the a -axis, $\epsilon_{1a} = (\phi_0/4\pi)H_{c1a}$, accounting for just the magnetic field energy density $b^2/8\pi$ and the kinetic energy density $(2\pi/c^2)(\lambda_b^2 j_y^2 + \lambda_c^2 j_z^2)$ yields the result, valid only to logarithmic accuracy,

$$H_{c1a} = (\phi_0/4\pi\lambda_b\lambda_c)\ln\kappa_a. \quad (3)$$

A more accurate, analytic expression for the magnetic field of an isolated vortex in the vicinity of the core, as well as for ϵ_{1i} and H_{c1i} , can be obtained by extending the variational model of Ref. 24 to the anisotropic case. In this approach, one takes a variational trial function for the order parameter of the form $f = \rho/R'$, where $\rho' = [(y/\lambda_c)^2 + (z/\lambda_b)^2]^{1/2}$, $R' = \{\xi_v'^2 + (y/\lambda_c)^2 + (z/\lambda_b)^2\}^{1/2}$, and ξ_v' is a variational core radius parameter of order $1/\kappa$. With this Ansatz, the solution of the second Ginzburg-Landau equation is²³⁻²⁴

$$b_x(y, z) = (\phi_0/2\pi\lambda_b\lambda_c)K_0(R') \quad (4)$$

when $\kappa \gg 1$. When this result and $f = \rho/R'$ are substituted back into the Ginzburg-Landau free energy functional to minimize the energy per unit length of vortex, all the integrals can be performed analytically and the energy is minimized with $\xi_v' = \sqrt{2}/\kappa_a$ if $\kappa_a \gg 1$, yielding

$$H_{c1a} = (\phi_0/4\pi\lambda_b\lambda_c)[K_0(\sqrt{2}/\kappa_a) + 3/4], \quad (5)$$

or, keeping only the leading terms in an expansion in powers of $1/\kappa_a$.

$$H_{c1a} = (\phi_0/4\pi\lambda_b\lambda_c)(\ln\kappa_a + 0.52). \quad (6)$$

The above variational calculation, however, slightly overestimates the energy per unit length of the vortex. As shown in Ref. 25, numerical solutions of the Ginzburg-Landau equations show that the constant term is not 0.52 but 0.497. Note that, if the vortex is centered along the y - or z -axis, the corresponding expressions for b_j and H_{c1j} can be obtained by cyclic permutation ($x \rightarrow y \rightarrow z \rightarrow x$ or $a \rightarrow b \rightarrow c \rightarrow a$).

For a discussion of the more complicated case for which the vortex is not along any of the principal axes, the reader is referred to Ref. 26.

At the upper critical field, the linearized Ginzburg-Landau equations can be solved for arbitrary angles (θ, ϕ) of the applied field $\mathbf{H} = H(\hat{x} \sin\theta \cos\phi + \hat{y} \sin\theta \sin\phi + \hat{z} \cos\theta)$. The magnitude of the upper critical field (at which bulk superconductivity is quenched) is⁹ $H_{c2}(\theta, \phi) = 2^{1/2} \kappa_{eff}(\theta, \phi) H_c = (\phi_0/2\pi\xi^2)[m_{eff}(\theta, \phi)]^{-1/2}$, where $\kappa_{eff}(\theta, \phi) = \kappa[m_{eff}(\theta, \phi)]^{-1/2}$ and

$$m_{eff}(\theta, \phi) = m_a \sin^2\theta \cos^2\phi + m_b \sin^2\theta \sin^2\phi + m_c \cos^2\theta. \quad (7)$$

When the applied field is directed along the a -, b -, and c -axes, we have $H_{c2a} = \phi_0/2\pi\xi_b\xi_c$, $H_{c2b} = \phi_0/2\pi\xi_c\xi_a$, and $H_{c2c} = \phi_0/2\pi\xi_a\xi_b$, respectively, as can be shown with the help of $m_1 m_2 m_3 = m_a m_b m_c = 1$ and $\xi_i = \xi/\sqrt{m_i}$.

3. JOSEPHSON-COUPLED BLOCKS OR LAYERS

Various consequences of modeling the high-temperature superconductors as Josephson-coupled blocks, layers, or subgrains¹⁷⁻²⁰ are currently under theoretical and experimental investigation. In order to bring out how magnetic fields penetrate a superconductor in such a picture, we analyze here a general model, sketched in Fig. 1, consisting of a periodic array of Josephson-coupled blocks. The blocks, rectangular parallelepipeds of dimensions a_1' , a_2' , and a_3' along the x , y , and z (a , b , and c) directions, are

arranged on an orthorhombic lattice with lattice parameters a_1 , a_2 , and a_3 . The areas of the junctions between the blocks normal to \hat{x} , \hat{y} , and \hat{z} are $A_1' = a_2'a_3'$, $A_2' = a_3'a_1'$, and $A_3' = a_1'a_2'$, while the corresponding areas of the sides of the unit cell are $A_1 = a_2a_3$, $A_2 = a_3a_1$, and $A_3 = a_1a_2$. The blocks are aligned with their symmetry axes along the x , y , and z directions, such that the corresponding intrinsic penetration depths are $\lambda_{10}(T)$, $\lambda_{20}(T)$, and $\lambda_{30}(T)$, while the intrinsic coherence distances are $\xi_{10}(T)$, $\xi_{20}(T)$, and $\xi_{30}(T)$. We assume that $a_i' \ll \lambda_0$, such that the local magnetic field within the unit cell penetrates each block almost uniformly. The blocks are Josephson-coupled with coupling energy $E_{Ji}(T) = (\pi/2e)I_0(T)$ across the junctions normal to the i direction. The supercurrent in the i direction across such a junction is $I_i = I_0 \sin\Delta\gamma_i$, where $I_0(T)$ is the maximum dc Josephson current,²⁷

$$I_0(T) = [\pi\Delta(T)/2eR_{in}] \tanh[\Delta(T)/2k_B T], \quad (8)$$

$\Delta(T)$ is the temperature-dependent gap parameter, R_{in} is the normal-state tunneling resistance across the junction, and $\Delta\gamma_i$ is the gauge-invariant phase difference across this junction.

Regardless of the strength of the Josephson coupling, the local magnetic field varies slowly on the scale of a_i . We wish to obtain a differential equation describing how superconductivity affects the slow spatial variation of \mathbf{B} , the magnetic flux density averaged over the unit cell. This equation, in combination with Ampere's law $(4\pi/c)\mathbf{J} = \nabla \times \mathbf{B}$, where \mathbf{J} is the current density averaged over the unit cell, will yield useful expressions for the supercurrent penetration depths λ_i along the three principal directions. Using a procedure similar to that used in Ref. 28, we obtain the desired equation by considering the magnetic flux $B_3(x, y)A_3$ in the z direction through the rectangle of area $A_3 = a_1a_2$ centered at $P(x, y)$. This flux can be expressed as a line integral of the vector potential \mathbf{a} around the rectangular contour 1-2-3-4-5-6-7-8-9-10-11-12-1 shown in Fig. 1. Within the blocks we first replace \mathbf{a} by $\mathbf{a}_s - (\phi_0/2\pi)\nabla\gamma$. We next make use of $\mathbf{a}_{sj} =$

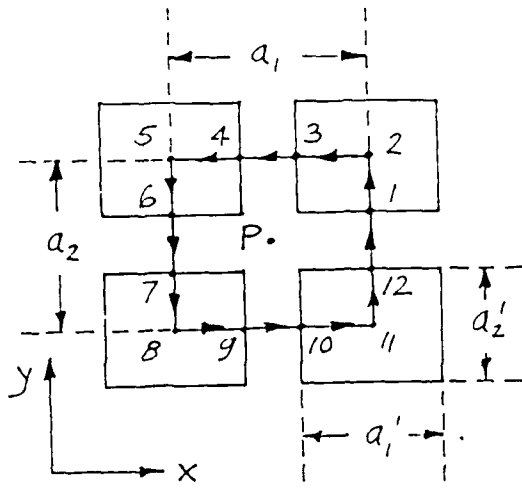


FIGURE 1
Josephson-coupled-block model.

$-(4\pi\lambda_0^2/c)j_i$, where $j_i A_i' = J_i A_i$, and the magnetic field is assumed to be sufficiently weak that $f = 1$. Expressing differences of J_i in adjacent blocks in terms of partial derivatives, we then obtain the following fluxoid quantization condition,

$$B_3 = -(\phi_0/2\pi A_3)(\Delta\gamma_{3,4} + \Delta\gamma_{6,7} + \Delta\gamma_{9,10} + \Delta\gamma_{12,1}) + (4\pi/c)[(\lambda_{10}^2 a_1' A_1/a_1 A_1')\partial J_1(x,y)/\partial y - (\lambda_{20}^2 a_2' A_2/a_2 A_2')\partial J_2(x,y)/\partial x], \quad (9)$$

where, for example, the gauge-invariant phase difference across junction 9,10 is

$$\Delta\gamma_{9,10} = \gamma_9 - \gamma_{10} - (2\pi/\phi_0) \int_9^{10} \mathbf{dl} \cdot \mathbf{a}, \quad (10)$$

the line integral being taken directly across the junction.

Since $\Delta\gamma_{3,4} = -\Delta\gamma_1(x,y+a_2/2)$, $\Delta\gamma_{6,7} = -\Delta\gamma_2(x-a_1/2,y)$, $\Delta\gamma_{9,10} = \Delta\gamma_1(x,y-a_2/2)$, and $\Delta\gamma_{12,1} = \Delta\gamma_2(x+a_1/2,y)$, we also may write

$$B_3 = (\phi_0/2\pi A_3)[a_2\partial\Delta\gamma_1(x,y)/\partial y - a_1\partial\Delta\gamma_2(x,y)] + (4\pi/c)[(\lambda_{10}^2 a_1' A_1/a_1 A_1')\partial J_1(x,y)/\partial y - (\lambda_{20}^2 a_2' A_2/a_2 A_2')\partial J_2(x,y)/\partial x]. \quad (11)$$

For weak fields and small current densities, we may linearize the Josephson current equation (replace $\sin\Delta\gamma$ by $\Delta\gamma$). Substitution of $J_i(x,y) = J_{0i}\Delta\gamma_i(x,y)$, where $J_{0i}(T) = I_{0i}(T)/A_i$, into the above equation then yields

$$B_3 = (4\pi/c)(\lambda_1^2\partial J_1/\partial y - \lambda_2^2\partial J_2/\partial x), \quad (12)$$

where

$$\lambda_i^2 = \lambda_{0i}^2 a_i' A_i/a_i A_i' + c\phi_0/8\pi^2 a_i J_{0i}. \quad (13)$$

Corresponding expressions for B_1 and B_2 can be obtained from the above by cyclic permutation. From these expressions and Ampere's law, one may show that if \mathbf{J} flows along only one of the three principal axes, only the λ_i along that axis determines its spatial variation. For example, if $\mathbf{J} = J_3\hat{z}$, then

$$\partial^2 J_3/\partial x^2 + \partial^2 J_3/\partial y^2 = J_3/\lambda_3^2. \quad (14)$$

To discuss the limiting cases of the expression for λ_i , note that if the junction barrier thicknesses shrink to zero and $J_{0i} \rightarrow \infty$, then $a_i' \rightarrow a_i$ and $A_i' \rightarrow A_i$. Thus $\lambda_i \rightarrow \lambda_{0i}$ in the strong-Josephson-coupled limit. On the other hand, if $J_{0i} \ll c\phi_0 A_i/8\pi^2 \lambda_{0i}^2 A_i a_i'$, we have $\lambda_i = (c\phi_0/8\pi^2 a_i J_{0i})^{1/2}$ in the weak-Josephson-coupling limit.

If the intrinsic normal-state resistivity within a given block along the i -axis is ρ_{0i} , then the effective resistivity of the array of blocks, which are connected in series with the tunnel resistances R_{in} , is

$$\rho_i = \rho_{0i} a_i' A_i/a_i A_i' + R_{in} A_i/a_i. \quad (15)$$

In the limit when $R_{in} \ll \rho_{0i} a_i' A_i'$, which can occur in the strong-Josephson-coupled limit, the junction resistance makes a small contribution to the overall resistivity, while in the opposite limit when $R_{in} \gg \rho_{0i} a_i' A_i'$, the junction resistance dominates the expression for ρ_i .

If the superconducting blocks are in the clean limit, there is no relation between ratios of the λ_{0i} 's and the ρ_{0i} 's. Similarly, for an array of clean-limit blocks,

there is no relation between ratios of the λ_i 's and the ρ_i 's. However, in the weak-coupling limits for which $R_{in} \gg \rho_0 a_i / A_i$ and $J_0 \ll c \phi_0 A_i / 8 \pi^2 \lambda_{i0}^2 A_i a_i$, the Ambegaokar-Baratoff theory²⁷ gives the following relation between λ_i and ρ_i :

$$\lambda_i^2 = \pi c^2 \rho_i / 4 \pi^2 \Delta(T) \tanh[\Delta(T) / 2 k_B T], \quad (16)$$

which agrees exactly with the corresponding result obtained from the BCS theory in the dirty limit.^{29,30} These results thus explain how it is possible for a highly anisotropic high-temperature superconductor to behave as if it were in the clean limit along one direction and in the dirty limit along another.

If we consider the case for which the blocks are strongly Josephson-coupled along the a and b directions but weakly coupled along the c direction, we obtain results similar to that of the closely related Lawrence-Doniach model.¹⁷ In this case the corresponding penetration depths along the a , b , and c directions are given by

$$\lambda_a^2 = \lambda_{a0}^2 a_3 / a_3', \quad (17a)$$

$$\lambda_b^2 = \lambda_{b0}^2 a_3 / a_3', \quad (17b)$$

$$\lambda_c^2 = \lambda_{c0}^2 a_3 / a_3 + c \phi_0 / 8 \pi^2 a_3 J_{30}, \quad (17c)$$

where a_3 is the lattice parameter along the c direction, a_3' is the effective thickness of the superconducting layer, and J_{30} is the maximum Josephson supercurrent density perpendicular to the layers.

The above derivations show how an anisotropic penetration depth tensor can be derived for an oriented array of Josephson-coupled blocks or layers whose small dimensions are less than the intrinsic penetration depth. The magnetic structure in such an array strongly resembles that in a homogeneous superconductor described by the London or Ginzburg-Landau theories with an anisotropic effective mass tensor. Far from the vortex cores the behavior is nearly the same in the two descriptions, but differences may occur in the vicinity of the vortex "core." In a homogeneous superconductor the $1/r$ dependence of the superfluid velocity around the vortex axis is cut off by order-parameter suppression ($f \approx r$) in the core,

such that the current density becomes proportional to r close to the vortex axis. Whether or not strong order-parameter suppression in the core occurs in a Josephson-coupled array depends upon the size of the effective coherence distance ξ_i relative to a_i . The results of Ref. 30 suggest that, while ξ_i may be close to ξ_{i0} with sufficiently strong Josephson coupling, the appropriate expression in the weak-Josephson-coupling limit is given near T_c by

$$\xi_i^2(T) = \pi^2 \pi \Delta^2(T) / 4 e^2 k_B T_c H_c^2(T) \rho_i. \quad (18)$$

The size of the vortex "core" is then given by the larger of ξ_i or $a_i/2$. If $\xi_i < a_i/2$, the suppression of the order parameter of the block is very small, the vortex axis sits in the Josephson junction between blocks,^{18,19} and the lower cutoff radius (in expressions such as that for H_{c1}) is $a_i/2$, not ξ_i .

4. CONCLUSION

In this paper, I have discussed several approaches being used to describe the intragranular magnetic structure in the mixed state of the high-temperature superconductors. Further extensions of these models are needed to provide a clear picture of the crossover between the regime in which the magnetic structure varies on length scales λ_i and ξ_i that are both larger than the linear dimensions of the discrete building blocks of the superconductor, and the regime in which the smallest length scales of the magnetic structure are set by the sizes of these building blocks.

ACKNOWLEDGMENTS

I thank V. G. Kogan, A. P. Malozemoff, R. A. Klemm, Z. Hao, and M. R. Beasley for stimulating discussions of the topics considered in this paper.

REFERENCES

1. J. G. Bednorz and K. A. Müller, Z. Phys. B (1986) 189.
2. J. R. Clem, Physica C 153-155 (1988) 50.

3. F. London, *Superfluids* (Dover, New York, 1961).
4. M. von Laue, *Theory of Superconductivity* (Academic Press, New York, 1952).
5. V. L. Ginzburg, *Zh. Eksp. Teor. Fiz.* 23 (1952) 236.
6. C. Caroli, P. G. de Gennes, and J. Matricon, *Phys. Kondens. Mater.* 1 (1963) 176.
7. L. P. Gor'kov and T. K. Melik-Barkhudarov, *Sov. Phys. JETP* 18 (1964) 1031.
8. D. R. Tilley, G. J. Van Gorp, and C. W. Berghout, *Phys. Lett.* 12 (1964) 305.
9. D. R. Tilley, *Proc. Phys. Soc. London* 85 (1965) 1977; 86 (1965) 289.
10. E. I. Katz, *Sov. Phys. JETP* 29 (1969) 897; 31 (1970) 787.
11. K. Takanaoka, *Phys. Status Solidi B* 68 (1975) 623.
12. R. A. Klemm and J. R. Clem, *Phys. Rev. B* 21 (1980) 1868.
13. V. G. Kogan, *Phys. Rev. B* 24 (1981) 1572.
14. V. G. Kogan and J. R. Clem, *Phys. Rev. B* 24 (1981) 2497.
15. A. V. Balatskii, L. I. Burlachkov, and L. P. Gor'kov, *Zh. Eksp. Teor. Fiz.* 90 (1986) 1478 [*Sov. Phys. JETP* 63 (1986) 866].
16. V. G. Kogan and J. R. Clem, *Jpn. J. Appl. Phys.* 26 (Suppl. 26-3) (1987) 1159.
17. W. Lawrence and S. Doniach, *Theory of layer structure superconductors*, in: *Proceedings of the Twelfth International Conference on Low Temperature Physics*, ed. E. Kanda (Academic Press of Japan, Kyoto, 1971), pp. 361-362.
18. R. A. Klemm, A. Luther, and M. Beasley, *Phys. Rev. B* 12 (1975) 877.
19. L. N. Bulaevskii, *Usp. Fiz. Nauk* 116 (1975) 449 [*Sov. Phys. Usp.* 18 (1976) 514].
20. T. Tsuneto, *J. Phys. Soc. Japan* 57 (1988) 3499.
21. G. J. Dolan, F. Holtzberg, C. Feild, T. R. Dinger, *Phys. Rev. Lett.* 62 (1989) 2184.
22. L. Ya. Vinnikov, I. V. Grigoryeva, L. A. Gurevich, and Yu. A. Osipyan, *Pis'ma Zh. Eksp. Teor. Fiz.* 49 (1989) 83.
23. R. P. Huebener, *Magnetic Flux Structure in Superconductors* (Springer-Verlag, Berlin, 1979).
24. J. R. Clem, *J. Low Temp. Phys.* 18 (1975) 427.
25. C.-R. Hu, *Phys. Rev. B* 6 (1972) 1756.
26. V. G. Kogan, *Anisotropy effects in high-temperature superconductors*, this volume.
27. V. Ambegaokar and A. Baratoff, *Phys. Rev. Lett.* 10 (1963) 486; 11 (1963) 104(E).
28. J. R. Clem, *Physica C* 153-155 (1988) 50.
29. D. Saint-James, E. J. Thomas, and G. Sarma, *Type-II Superconductivity* (Pergamon, Oxford, 1969).
30. J. R. Clem, B. Bumble, S. I. Raider, W. J. Gallagher, and Y. C. Shih, *Phys. Rev. B* 35 (1987) 6637.

HIGH RESOLUTION-ANGLE RESOLVED PHOTOEMISSION STUDIES OF HIGH TEMPERATURE SUPERCONDUCTORS

C. G. OLSON^{*}, R. LIU, D. W. LYNCH

Ames Laboratory[‡] and Department of Physics, Iowa State University, Ames, IA 50011

B. W. VEAL, Y. C. CHANG, P. Z. JIANG, J. Z. LIU, A. P. PAULIKAS

Argonne National Laboratory, Argonne, IL 60439

A. J. ARKO, R. S. LIST

Los Alamos National Laboratory, Los Alamos, NM 87545

Recent photoemission studies of Y 123 and Bi 2212 performed with high energy and angular resolution have provided detailed information on the nature of the states near the Fermi level. Measurements of the superconducting gap, band dispersion, and the density of states near the Fermi level in the normal state all support a Fermi liquid description of these materials.

1. INTRODUCTION

Historically, photoemission has had mixed success in determining the electronic structure of the high temperature superconductors. More recently, it has been shown¹ that it is important to cleave $\text{YBa}_2\text{Cu}_3\text{O}_{7-\delta}$ (Y 123) samples at low temperature to ensure that the surface probed by photoemission is characteristic of the bulk. The $\text{Bi}_2\text{Sr}_2\text{CaCu}_2\text{O}_8$ (Bi 2212) class of superconductors is much more stable at elevated temperature, but reduced temperatures prolong the useful life of a surface. Additionally, reduced Fermi level broadening is important in studying the details of band dispersion near the Fermi level. Spectra can be further simplified by angular (k space) resolution, high kinetic energy resolution, or the application of all three at the same time.

2. EXPERIMENTAL

Measurements were done at the Synchrotron Radiation Center^{*}, Stoughton, Wisconsin on the Ames/Montana State-ERG/Seya beamline². The photoemission spectrometer has two degree angular resolution and is capable of 20 meV electron resolution. The combined system resolution in Figs. 3 and 4 was 32 meV.

3. RESULTS

The spectra in Fig. 1 are taken in normal emission. In this geometry a shift in the binding energy of a peak as a function of photon energy represents dispersion along the direction normal to the ab plane. As can be seen in Fig. 1a for Bi 2212, there is minimal dispersion. The primary effects are a small shift of the 3.5 eV peak to lower binding energy

^{*} Some support for the presentation of this work relates to Department of Navy Grant N00014-89-J-1837 issued by the Office of Naval Research. The United States Government has a royalty-free license throughout the world in all copyrightable material contained herein.

[‡] The Ames Laboratory is operated for USDOE by Iowa State University under contract No. W-7405-eng-82.

^{*} The Synchrotron Radiation Center is supported by NSF under contract #DMR8601349.

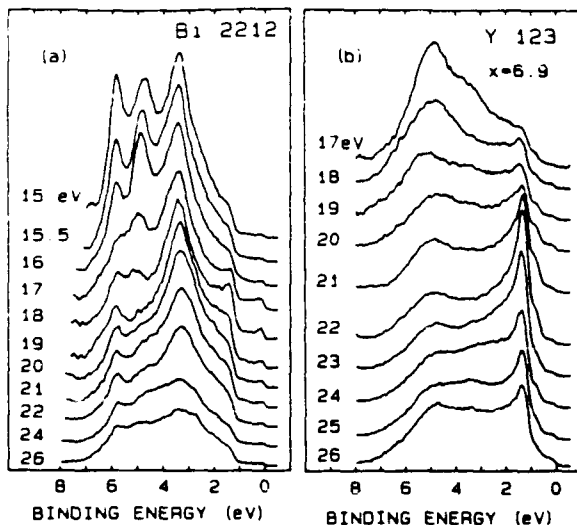


FIGURE 1
Photoemission energy distribution curves taken in normal emission for Bi 2212 (a) and Y 123 (b). The samples were cleaved and maintained at 20K. The spectra are normalized to incident photon flux.

with increasing photon energy and a larger shift of the 4.8 eV peak to higher binding energy. The small amount of dispersion in the z direction is not surprising in this highly two dimensional material. Dispersion in less well defined peaks is masked by the very strong intensity modulations due to matrix element effects. The enhancement near the Fermi level and at 1.5 eV for photon energies near 18 eV are only one of the strong selection rule effects.

Fig. 1b is a similar set of spectra for Y 123. Again, the two dimensionality of this material results in minimal dispersion in this geometry. There are indications of dispersion lower in the valence band, but the dominant features are the very strong matrix element effects. From these spectra, and others taken at other emission angles, it is clear that the strong enhancement of the 1.25 eV peak at a 22 eV photon energy is a matrix element effect and not an oxygen resonance.

Dispersion is much larger along directions in the ab plane. Fig. 2 are spectra for different emission angles and hence different k values along approximately the Γ -S direction. An initial state at 1.25 eV splits with one branch remaining at about 1.25 eV and the other moving deeper away from the zone center. Additional dispersion is seen in the lower part of the valence band. Finally, a band is seen dispersing through the Fermi level. In both Fig. 1 and 2, because of the moderate resolution (150 meV), emission near the Fermi level is largest when the band is actually well below E_f . High resolution data taken at the same time as the spectra in Fig. 2 show that the Fermi level crossing is at 12 degrees.

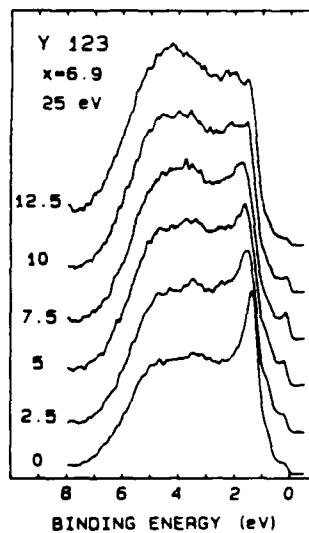


FIGURE 2
Angle resolved photoemission spectra along approximately the Γ -S direction, normalized to incident photon flux. The angle is relative to the sample normal.

For Bi 2212, emission near the Fermi level can be seen in much greater detail in the high resolution spectra of Fig. 3. As predicted by all band structure calculations, there is

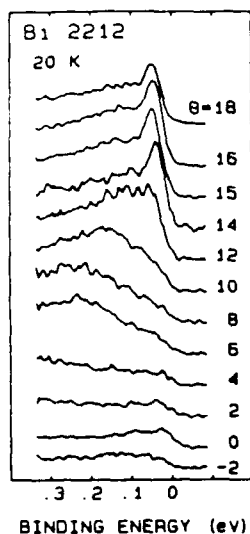


FIGURE 3

High resolution angle resolved spectra along approximately the Γ -M direction, normalized to incident flux.

minimal emission from the Fermi level near the zone center. The structure that is seen near normal emission in the figure probably comes from randomly oriented damaged areas at the edges of the sample. Increasing angles sample a line near the zone diagonal (Γ -M). A band is seen dispersing towards the Fermi level from at least 300 meV below E_f and then moving away from the Fermi level. This follows the calculated band³ qualitatively but the measured band appears much closer to the Fermi level than predicted. This is in qualitative agreement with Takahashi et.al.⁴

The measurements shown in Fig. 3 were taken at 20K, and the shape of the band near the Fermi level is distorted by the existence of a superconducting gap. Data reported in Ref. 5 were taken along a line parallel to that of Fig. 3, and include a point which is one of the few places where a band in the normal state crosses the Fermi level. The spectra⁵ in the normal and superconducting state are shown in

the upper part of Fig. 4. Modeling these spectra gave $2\Delta/KT_c = 7$, twice the weak coupling BCS value. In the bottom half of Fig. 4, the same normal state spectrum is compared to a platinum foil on the sample holder. The instrumental resolution (32 meV) is comparable to the Fermi level width at this temperature (34 meV). The measured Fermi levels are equivalent to within the resolution and noise of the experiment. A report by these authors of a more extensive experiment on the normal state Fermi level properties is in preparation, with the goal of placing quantitative limits on the possible value of RVB parameters.

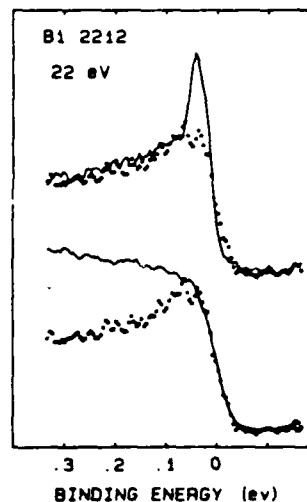


FIGURE 4

Upper: High resolution spectra showing modifications to the density at the Fermi level as a result of a superconducting gap. The solid curve is for 20K, and the dotted curve is for 90K; above the T_c of 82K. Lower: The same normal state density compared to a Pt density of states (solid line) at 90K.

4. CONCLUSIONS

High energy and angular resolution combined with low temperature is giving an increasingly detailed picture of the high temperature superconductors. Some of the detail, such as

the importance of matrix element effects, means a complete angle resolved study of the valence bands will be very time consuming. Fortunately, increased resolution simplifies other parts of the study. We have determined that bands cross the Fermi level at relatively few points in the zone. By isolating those points from the background we have determined the superconducting gap, and determined that the spectral density in the normal state looks like an ordinary metal. Increasingly, Y 123 and Bi 2212 are looking like traditional Fermi liquid materials.

REFERENCES

1. A.J. Arko et. al., J. Mag. Magn. Mat. 75 (1988) L1.
2. C.G. Olson, Nuc. Inst. Methods in Physics Research A266 (1988) 205.
3. S. Massidda, J. Yu, and A.J. Freeman, Physica C 52 (1988) 251.
4. T. Takahashi et. al., Phys. Rev. B39 (1989) 6636.
5. C.G. Olson et.al., Science (1989) in press.

SPIN FLUCTUATIONS, SPIN BAGS AND THE HIGH T_c SUPERCONDUCTIVITY

J.R. SCHRIEFFER, X.G. WEN and S.C. ZHANG*

Institute for Theoretical Physics, University of California, Santa Barbara, CA 93106

The magnetic properties of the half-filled one band Hubbard model is studied within the random phase approximation (RPA) above the mean field spin-density-wave (SDW) background. The spin wave spectrum and the sublattice magnetization are shown to interpolate smoothly between the weak and strong coupling limits. A hole in the SDW background is self-trapped in a region of reduced SDW amplitude and forms an object which we call the spin bag. The attraction among the two holes results due to the tendency to share the region of reduced SDW amplitude. A detailed calculation based on the RPA above the SDW background support this picture. The symmetries and the nodes of the resulting pairing gap are discussed.

1. INTRODUCTION

One of the characteristic features of the high T_c superconductors is the antiferromagnetic correlations present both in the insulating and in the metallic phases.¹ Many theories are thus based on the point of view that this observed antiferromagnetic correlation is intimately related to the occurrence of the superconductivity. There are two different ways to approach the magnetic phase based on the single band Hubbard model, the localized Mott limit where the problem can be mapped onto a Heisenberg model and the itinerant limit where the magnetic order arises due to the fermi surface nesting. We shall present a quantitative analysis based on the RPA above the SDW background to show that physical properties actually interpolate smoothly between these two seemingly opposite limits.² The doped metallic phase can also be approached from two different directions, with one starting from the para-

magnetic phase where one postulates a new spin liquid like magnetic order and the other starting from the antiferromagnetic phase where one assumes that the length scale of the antiferromagnetic order to be larger than the other length scales in the problem. One expects that physical properties should also interpolate smoothly between these two limits although a quantitative demonstration is still lacking. In our approach,² we shall discuss the problem starting from the antiferromagnetic phase.

2. MAGNETIC PROPERTIES AT HALF-FILLING

At half-filling and strong coupling ($U \gg t$), the Hubbard model maps onto the Heisenberg model with $J \sim t^2/U$. The numerical investigations show that the ground state is Néel ordered.³ The spin wave velocity is of the order of J and the quantum fluctuations reduce the sublattice magnetiza-

* Some support for the presentation of this work relates to Department of Navy Grant N0014-89-J-1837 issued by the Office of Naval Research. The United States Government has a royalty-free license throughout the world in all copyrightable material contained herein.

tion to $0.6\mu_B$ from the classical value of $1\mu_B$.⁴ In the weak coupling limit ($U \ll t$), the fermi surface is a perfect square and this nesting property leads to an instability of the free fermi surface and to the formation of a SDW ground state. In this limit, the spin wave velocity is of the order of the fermi velocity t and the sublattice magnetization is exponentially small. Clearly the ground states in both limits have the same symmetry and other qualitative features, the question is how physical quantities interpolate between these two limits. We performed a calculation based on the RPA above the mean field SDW ground state to extract the spin wave velocity from the gapless pole in the transverse susceptibility.² The resulting spin wave velocity indeed interpolates smoothly between the weak and the strong coupling limits. Furthermore, both the mean field and the fluctuation reduced sublattice magnetization can be worked out within this formalism and again we found smooth behavior between the two limits. Actually the fluctuation reduced sublattice magnetization we obtained compare well with the Monte Carlo results of Hirsch and Tang.³

3. THE SPIN BAG AND SUPERCONDUCTIVITY

When a hole is injected to the rigid SDW background, it costs a minimal energy of the SDW gap Δ_{SDW} . The system therefore has the tendency of reducing the SDW amplitude in the vicinity of the hole as to lower the self-energy. The gain in self-energy of the hole is balanced by the cost of the exchange energy and these two competing effects lead to the self-consistent formation of an object which we call a spin bag.² The size of the spin bag is of the order of the SDW coherence length $\xi_{SDW} \sim t/\Delta_{SDW}$ and is about three to four lattice spacing. The shape of the spin bag can be round or cigar like depending on the location in fermi surface. All these quali-

tative features are observed in the numerical variational calculation by Su.⁵ From this reasoning one concludes that two holes attract each other because of the tendency to share the region of reduced SDW amplitude as to lower the cost of exchange energy. We believe that this is the basic mechanism by which the superconducting pairing occurs.

The above qualitative picture is supported by a detailed dynamic calculation of the pairing interaction mediated by the collective modes of the SDW background.^{2,6} These collective modes are: the charge fluctuation, the spin orientation and the spin amplitude fluctuations. There is no significant enhancement in the charge fluctuation channel since one is dealing with the positive U Hubbard model. The spin orientation fluctuation (the spin wave) is an important low energy mode. However it couples to the holes with a vertex which vanishes in the small doping limit and can be neglected in the Born approximation. The most important mode is the spin amplitude fluctuation which couples to the holes with unit strength even in the small doping limit and according to our previous argument, it is responsible for the formation of the spin bag.

The qualitative features of the spin amplitude fluctuation are: 1) attractive for small momentum transfer and repulsive for momentum transfer near $\vec{Q} = (\pi, \pi)$ the nesting wave vector; 2) the spectral weight is peaked around Δ_{SDW} , which serves as a frequency cut-off similar to the Debye frequency in the phonon problem. For small doping, holes form "pocket" at the magnetic zone boundary, concentrated either around $(0, \pi)$ or $(\frac{\pi}{2}, \frac{\pi}{2})$. These features of the hole fermi surface combined with the properties of the spin amplitude fluctuation mode lead to a pairing gap that has either a d -wave or p -wave like symmetry but the pairing gap has no nodes at the hole fermi surface in either case.

4. CONCLUSION

Starting from the mean field SDW ground state, we demonstrated that RPA fluctuations describe the magnetic properties correctly in both the localized and the itinerant limits. Upon doping, the spin amplitude fluctuation is the dominant mode that couples to the hole and leads to the formation of the spin bag. The properties of the hole fermi surface and the spin amplitude mode are such that the resulting pairing gap is nodeless over the hole fermi surface.

ACKNOWLEDGEMENT

We would like to acknowledge helpful discussions with H. Nakanishi, D.J. Scalapino and K. Schönhammer. This work was supported in part (J.R.S. and S.C.Z.) by the NSF grant DMR85-17276 and also (X.G.W.) PHY82-17853, supplemented by funds from NASA.

REFERENCES

1. G. Shirane, *et al.*, Phys. Rev. Lett. **59** (1987) 1613; J. Transquada, *et al.*, Phys. Rev. Lett. **60** (1988) 156; K.B. Lyons, *et al.*, Phys. Rev. **B37** (1988) 2353; K.B. Lyons, *et al.*, Phys. Rev. Lett. **60** (1988) 732; R.J. Birgeneau, *et al.*, Phys. Rev. **B38** (1988) 6614.
2. J.R. Schrieffer, X.G. Wen and S.C. Zhang, Phys. Rev. Lett. **60** (1988) 944; Phys. Rev. **B39** (1989) 11663.
3. J.D. Reger and A.P. Young, Phys. Rev. **B37** (1988) 5978; J.E. Hirsch and S. Tang, preprint.
4. P.W. Anderson, Phys. Rev. **86** (1952) 694.
5. W.P. Su, Phys. Rev. **B37** (1988) 9904.
6. Z.Y. Weng, T.K. Lee and C.S. Ting, Phys. Rev. **B38** (1988) 6561; G. Vignale and K.S. Singwi, Phys. Rev. **B39** (1989) 2956.

Probing Magnetism and Superconductivity of High- T_c Systems with Positive Muons

Y.J. Uemura¹, L.P. Le¹, G.M. Luke¹, B.J. Sternlieb¹,
J.H. Brewer², R. Kadono², R.F. Kieff², S.R. Kreitzman², and T.M. Riseman²

1. Department of Physics, Columbia University, New York City, New York 10027, U.S.A.
2. TRIUMF and Department of Physics, University of British Columbia, Vancouver, B.C., V6T 2A3, Canada

Abstract

Recent results from our μ SR experiments on high- T_c systems are presented. We describe studies of static magnetic order in hole-doped and electron-doped systems, correlations between T_c and n_s/m^* (carrier density / effective mass) in hole-doped superconducting cuprates, the temperature dependence of the penetration depth in c-axis oriented sintered ceramic of $YBa_2Cu_3O_7$, as well as the detection of flux pinning phenomena by μ SR.

Introduction

Positive muon spin relaxation (μ SR) has been very useful for the study of high- T_c systems¹⁻³. With this technique, one can measure static magnetic order, even with very small and random moments, and study details of magnetic phase diagrams. The magnetic field penetration depth in superconductors, determined directly by μ SR, has revealed various aspects of superconducting energy gap, carrier density, as well as flux pinning. In this paper, we review recent progress of our μ SR experiments at TRIUMF (Vancouver) to demonstrate these features of μ SR.

Experimental aspects

The principle of μ SR technique has been described in earlier review papers^{1,2} and other literatures⁴. The polarized positive muon beam is stopped in a specimen (typically 1 ~ 2 cm in diameter, 1 ~ 2 mm thick), and time histograms of muon decay events are recorded, one by one, by positron counters placed at forward (F) and backward (B) directions with respect to the initial muon spin direction. Since positrons are emitted preferentially along the muon spin direction, the time evolution of the muon spin direction and polarization can be directly observed via the F/B angular asymmetry of the positron time spectra. This measurement can be performed either in zero field (ZF- μ SR) or by applying a transverse external magnetic field (TF- μ SR). After stopping almost instantaneously (typically within $\sim 10^{-11}$ sec) at an interstitial site, the μ^+ generally stays at rest in oxides during its life (mean life time of μ^+ is 2.2 μ sec), probing magnitude, randomness, and fluctuations of local magnetic fields at the interstitial site, analogously to an implanted proton.

Magnetic order — hole-doped systems

We previously reported μ SR studies in La_2CuO_{4-y} (ref. 5) and $YBa_2Cu_3O_x$ (ref. 6) which established: (1) The Néel temperature is reduced sharply with increasing Oxygen concentration, and static magnetic order disappears near the concentration where the superconductivity appears; (2) the static moment of Cu in the antiferromagnetic phase does

not depend much on the Néel temperature. There were, however, a report by Weidinger *et al.*⁷ that the static magnetic order remains deep in the superconducting phase, e.g., even in $La_{1.85}Sr_{0.15}CuO_4$. To clarify whether or not this is the intrinsic property, we have performed⁸ zero-field μ SR measurements on a $La_{1.85}Sr_{0.15}CuO_4$ specimen made by spray-dry method as well as on carefully annealed sintered specimens of $YBa_2Cu_3O_x$ at $T = 0.02$ K.

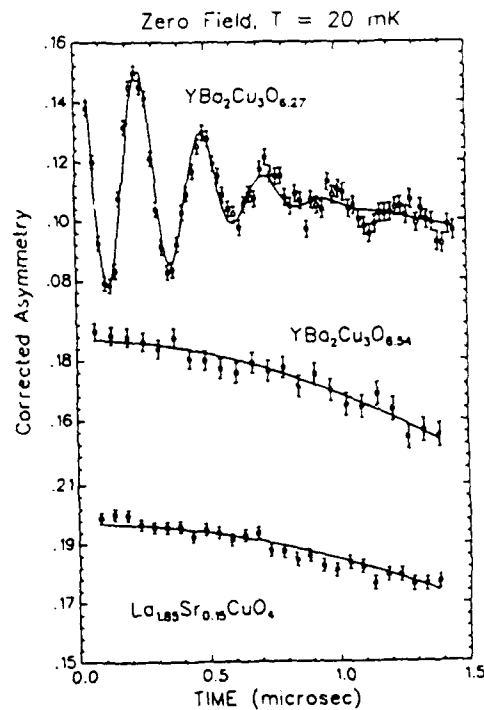


Fig. 1. Zero-field μ SR spectra at $T = 20$ mK in $YBa_2Cu_3O_x$ with $x = 0.27$ (non-superconducting), $x = 6.54$ (superconducting), and in $La_{1.85}Sr_{0.15}CuO_4$ (from Kieff *et al.*⁸).

Figure 1 shows the time dependence of the muon spin polarization in these systems. In non-superconducting $YBa_2Cu_3O_{6.27}$, the muon spin precesses around the static internal field from nearby Cu moments, thus confirming static magnetic order. In contrast, the time spectra of superconducting specimens, $YBa_2Cu_3O_{6.54}$ and $La_{1.85}Sr_{0.15}CuO_4$, showed only very slow depolarization, whose rate can be accounted for by nuclear dipolar fields. This rules out the existence of static magnetic order (with the accuracy better than $0.01 \mu_B$ per Cu) in good superconducting specimens. This demonstrates that static magnetic order is not an intrinsic property of superconducting hole-doped high- T_c systems. The results of ref. 7 may be due to inhomogeneity of the specimen.

Magnetic order — electron-doped systems

We have also performed⁹ μ SR studies on various specimens of the electron-doped system $Nd_{2-x}Ce_xCuO_4$ ($0.0 \leq x \leq 0.18$; reduced and non-reduced). Figure 2 shows typical zero-field μ SR spectra. The pure parent system Nd_2CuO_4 exhibits static magnetic order with $T_N = 250K$. We have also found a signature of spin re-orientation at $T \sim 80K$ and $T \sim 30K$ in this system, due to the instability of spin directions in the tetragonal crystal structure. The fast spin depolarization in non-superconducting $Nd_{1.9}Ce_{0.1}CuO_4$ confirms that the static magnetic order extends in the doped system. In contrast, the superconducting specimen with $x = 0.16$, reduced, does not show any signature of static order of Cu spins above $T = 5K$.

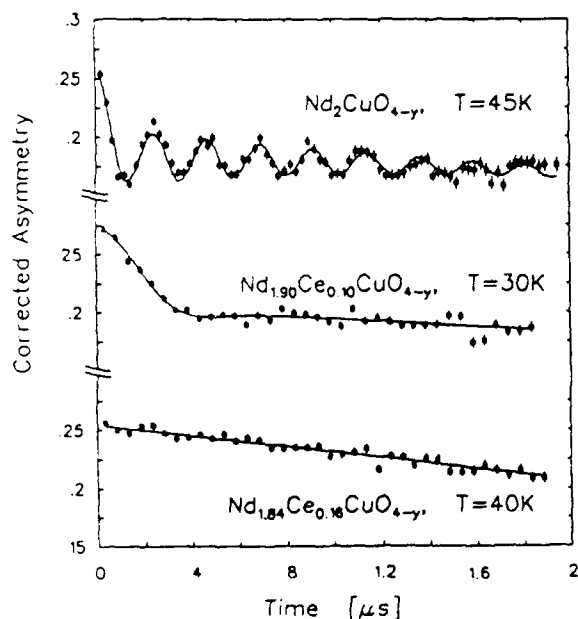


Fig. 2. Zero-field μ SR spectra in the electron-doped system $Nd_{2-x}Ce_xCuO_4$ with $x = 0.0$ and 0.1 (non-superconducting), and $x = 0.16$ (superconducting) reduced ceramic specimens (from Luke et al.⁹).

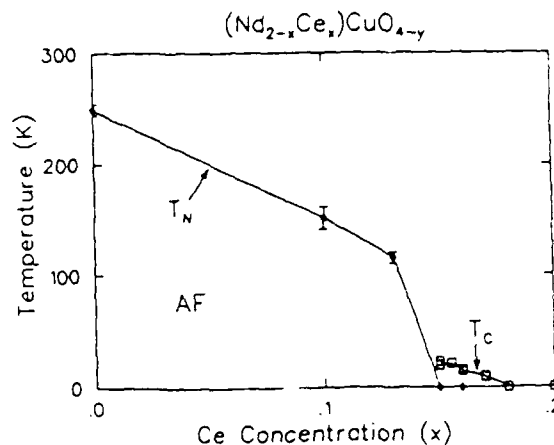


Fig. 3. Magnetic and superconducting phase diagram of $Nd_{2-x}Ce_xCuO_4$. Magnetic phase boundary is determined by μ SR, while superconducting phase boundary by resistivity (from Luke et al.⁹).

Based on these results, we obtained the magnetic phase diagram as shown in Fig. 3. Similarly to hole-doped systems, the static magnetic order disappears around the concentration where the superconductivity appears. Here again, there is no clear evidence for the intrinsic coexistence of superconductivity and the magnetic order of Cu spins. In the electron-doped systems, the magnetic order extends to much higher impurity concentration ($x \sim 0.15$) compared to the case of the hole-doped 214 system. A hole doped in the CuO_2 plane is believed to stay at the oxygen site as O^{1-} , creating a frustrated bond within the $Cu \uparrow O^{2-} Cu \downarrow$ antiferromagnetic network. The electron carrier, in contrast, goes to the Cu atom, making it as non-magnetic $Cu \uparrow \downarrow$. Thus the electron doping is equivalent to dilution of the magnetic moments, which has much milder effect in destroying spin order compared to frustration. This argument qualitatively explains the extended region of the antiferromagnetic phase in Fig. 3.

Penetration depth — T_c v.s. n_s/m^*

To measure the magnetic field penetration depth λ , we apply transverse external magnetic field H_{ext} ($H_{c1} < H_{ext} < H_{c2}$; typically $H_{ext} = 2 - 20kG$), and observe the depolarization of the muon spin precession: for simplicity¹⁰, one usually assumes the Gaussian relaxation function $\exp(-\sigma^2 t^2/2)$ to define the relaxation rate σ . Figure 4 shows examples of the temperature dependence $\sigma(T)$ observed in two different high- T_c superconductors, measured by cooling in H_{ext} (field cooling). In the superconducting state, H_{ext} penetrates the specimen, forming a lattice of flux vortices. The local field B becomes inhomogeneous: B is largest at the core, while smallest in the midpoint between adjacent flux cores. As an ensemble average signal from many muons stopped at different locations with respect to the flux lattice, μ SR samples the field distribution in the vortex state. The London equation leads to $\Delta B \propto 1/\lambda^2$, where $\Delta B \equiv (\langle (B - \langle B \rangle)^2 \rangle)^{1/2}$.

Therefore, by measuring the relaxation rate σ , one can determine the penetration depth, which is related to the superconducting carrier density n_s , divided by the effective mass m^* as

$$\sigma \propto \Delta B \propto 1/\lambda^2 \propto n_s/m^*.$$

We performed¹¹ the measurements of $\sigma(T)$ on more than 20 specimens (unoriented, sintered disks) of various high- T_c superconductors. Assuming the angular averaging process for anisotropy of λ to be the same for different specimens, one can regard $\sigma(T \rightarrow 0)$ to represent the ground state values of n_s/m^* of each system. We selected the results from specimens which show sharp changes of σ at T_c with greater than a 90 % superconducting volume fraction. Figure 5 shows T_c and $\sigma(T \rightarrow 0)$, both determined by μ SR. With increasing hole doping, T_c initially increases, following a linear relation with n_s/m^* universal to systems with single, double, and triple CuO_2 layers. Then, T_c shows saturation and suppression in the heavily-doped region. Recently, we have added¹² two points on $(\text{Y}_{1-x}\text{Pr}_x)\text{Ba}_2\text{Cu}_3\text{O}_7$ with $x=0.15$ and 0.3 in Fig. 4, which agree quite well with the results on $\text{YBa}_2\text{Cu}_3\text{O}_x$. This suggests that T_c is determined solely by the carrier density, regardless of the source of the doping.

μ SR is unique in providing information directly related to the superconducting carrier density. The results in Fig. 5 should be explained by successful theory of high- T_c superconductivity. The horizontal axis $\sigma \propto n_s/m^*$ is proportional to Fermi energy ϵ_f of non-interacting 2-dimensional electron gas. Therefore, one possible interpretation is to view the straight line as indicating $T_c \propto \epsilon_f$, which is not expected in the weak-coupling BCS model but is conceivable when the energy scale of the pairing interaction is larger than ϵ_f (i.e., no retardation¹³).

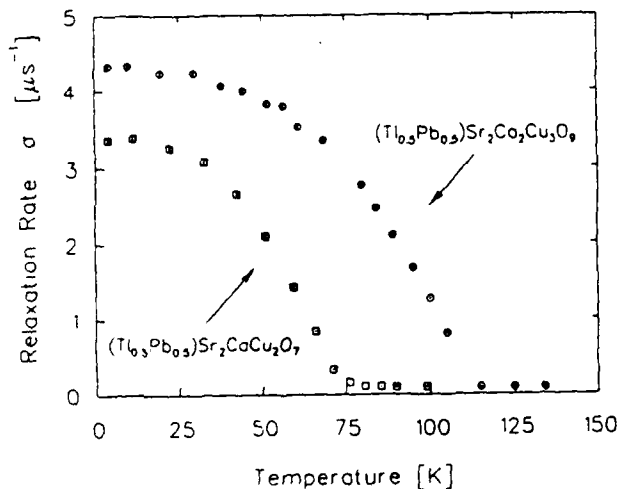


Fig. 4. The temperature dependence of the muon spin relaxation rate σ observed in superconducting Tl-Pb-Sr-Ca-Cu-O systems [with double and triple CuO_2 layers] in a transverse external magnetic field of 2.5 kG (from Uemura et al.¹¹).

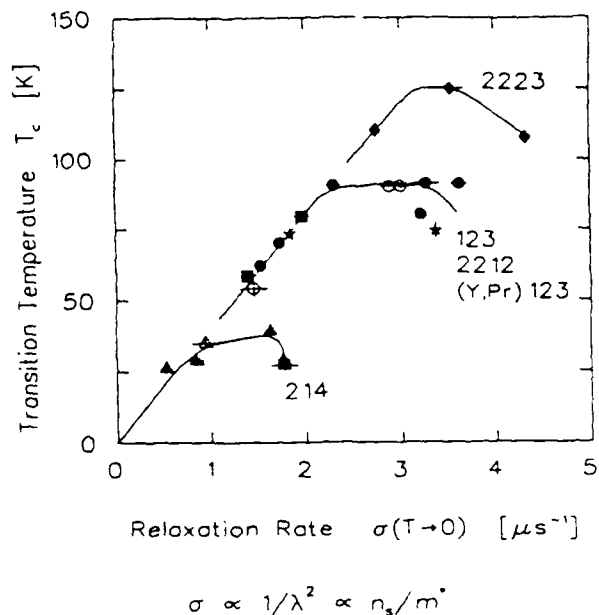


Fig. 5. The superconducting transition temperature T_c plotted versus low-temperature muon spin relaxation rate $\sigma(T \rightarrow 0)$ of various planar hole-doped high- T_c cuprates (see ref. 11 for details). The closed square points represent $(\text{Y}_{1-x}\text{Pr}_x)\text{Ba}_2\text{Cu}_3\text{O}_7$ with $x = 0.15$ and 0.3 . (from Uemura et al.¹¹).

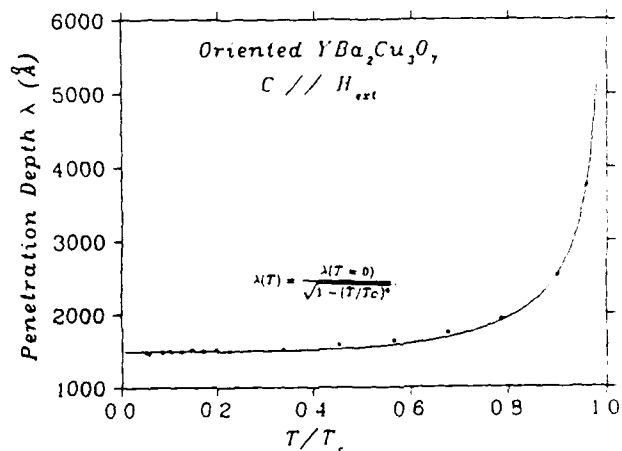


Fig. 6. The temperature dependence of the magnetic field penetration depth λ_{\parallel} derived from the muon spin relaxation rate σ in a c-axis oriented sintered ceramic specimen of $\text{YBa}_2\text{Cu}_3\text{O}_7$ with the external field $H_{\text{ext}} = 13\text{kG}$ applied parallel to the c-axis. The solid line represents the fit to the two-fluid model. (from Uemura et al.¹).

Penetration depth — energy gap

Thermal excitations across the energy gap destroy the Cooper pairs, reduce n_s , and make the penetration depth at finite temperatures longer than $\lambda(T=0)$. Figure 6 shows $\lambda(T)$ determined in a *c*-axis oriented ceramic specimen of $YBa_2Cu_3O_7$ with $H_{ext} \parallel c$ -axis¹. $\lambda(T)$ agrees reasonably well with the two fluid model, indicating that the energy gap is finite without any detectable anomalous zeros. Essentially the same results are obtained on non-oriented specimens of all the other hole-doped planer systems (214, 2212, 123, 2223, and similar systems). Experiments are now underway to extend the μ SR measurements of $\lambda(T)$ to heavy-fermion and organic superconductors.

Flux pinning

Recently, we have found¹⁴ that μ SR can also detect flux pinning phenomena. See Fig. 7. When an external field is applied above T_c followed by field cooling (FC), there is no anomaly in the $\sigma(T)$ curve. With H_{ext} applied perpendicular to the face of the thin disk specimen, the total magnetic induction B is the same above and below T_c . Then, the flux vortex does not have to move any macroscopic distance, and the FC μ SR results are insensitive to flux pinning. In contrast, if one applies the external field after cooling in zero field (ZFC), the flux vortices must move macroscopic distances. If the flux is trapped during this motion, the resulting field distribution would be more inhomogeneous than the case of FC. Therefore, the difference between the FC and ZFC data in Fig. 7 shows that the flux pinning takes place below $T \sim 30K$ in the Bi 2212 system. This pinning temperature agrees very well with those found in resistivity and mechanical measurements¹⁵. This serves to confirm that the phenomena observed in these bulk measurements were indeed related to the motion of the flux vortex.

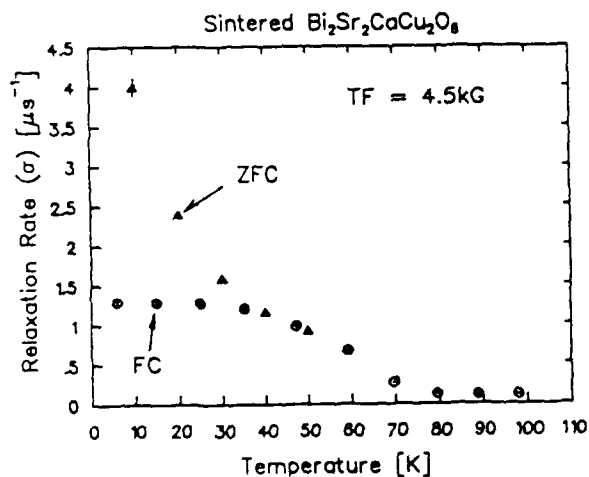


Fig. 7. Comparison of the muon spin relaxation rate σ in a sintered ceramic specimen of $Bi_2Sr_2CaCu_2O_8$ measured with the field cooling (FC) and zero-field cooling (ZFC) procedures with the external field of 4.5 kG. The difference between FC and ZFC results below $T = 30K$ is due to flux pinning. (from Sternlieb *et al.*¹⁴).

Conclusions

The temperature/concentration phase diagrams of planar cuprate high- T_c systems, obtained by μ SR both in hole-doped and electron-doped compounds, indicate the existence of critical carrier concentrations which separate the semiconducting region with statically ordered Cu moments and the superconducting region with metallic normal-state conductivity. The boundary between these two regions is very sharp, and there is no signature of intrinsic coexistence. This strongly suggests that the mechanism of high- T_c superconductivity is intimately related to magnetism. The universal correlation between n_s/m^* and T_c in the superconducting state, as well as the existence of finite energy gap without anomalous zeros, will be useful for the determination of pairing and condensation mechanisms. Ongoing μ SR experiments will continue to provide information on these aspects as well as on flux pinning phenomena in various superconducting systems.

Acknowledgement

We thank J.F. Caloran, W. Hardy, P. Mulhern, B.X. Yang, A.W. Sleight, M.A. Subramanian, J. Gopalakrishnan, S. Uchida, H. Takagi, Y. Tokura, Y. Hidaka, T. Murakami, H. Hart, K.W. Lay, D.C. Johnston, C.L. Chien, M.Z. Cieplak, Gang Xiao, V.Y. Lee, B.W. Statt, M.B. Maple, M.K. Wu and G. Saito for providing high-quality specimens and collaborating on the μ SR experiments, J. Kempton, W.J. Kossler, C.E. Stronach, K. Kakurai and C.S. Seaman for collaboration on μ SR, and R.J. Birgeneau, V.J. Emery, T.D. Lee, A.M. Portis and G. Shirane for stimulating discussions.

References

1. Y.J. Uemura *et al.*, J. Phys. (Paris) 49 Colloq., C8-2087 (1988).
2. Y.J. Uemura, J. Appl. Phys. 64, 6087 (1988).
3. For high- T_c studies of various μ SR groups, see also, N. Nishida *et al.*, J. Phys. Soc. Japan 57, 599 (1988); D.R. Harshman *et al.*, Phys. Rev. B38 852 (1988); A. Schenck, Physica C153-155, 769 (1988); H. Keller *et al.*, *ibid.* 71; J.I. Budnick *et al.* Europhys. Lett. 5, 651 (1988); and references therein.
4. A. Schenck, *Muon Spin Rotation*, Adam Hilger, Bristol (1986); Y.J. Uemura *et al.*, Phys. Rev. B31, 546 (1985).
5. Y.J. Uemura *et al.*, Phys. Rev. Lett. 59, 1045 (1987); Physica C153-155, 769 (1988).
6. J.H. Brewer *et al.*, Phys. Rev. Lett. 60, 1073 (1988).
7. A. Weidinger *et al.*, Phys. Rev. Lett. 62, 102 (1989).
8. R.F. Kiefl *et al.*, this conference.
9. G.M. Luke *et al.*, Nature 338, 49 (1989), and this conference.
10. For details of the line shapes, see T.M. Riseman, M.Sc. Thesis (1989).
11. Y.J. Uemura *et al.*, Phys. Rev. Lett. 62, 2317 (1989).
12. C.S. Seaman *et al.*, to be published.
13. V.J. Emery and G. Reiter, Phys. Rev. B38, 4547 (1988).
14. B.J. Sternlieb *et al.*, this conference.
15. T.T.M. Palstra *et al.*, Phys. Rev. Lett. 61, 1662 (1988); P.L. Garrinel *et al.*, *ibid.* 1666.

CRYSTAL CHEMISTRY OF OXIDE SUPERCONDUCTORS

Arthur W. SLEIGHT

Department of Chemistry, Oregon State University, Corvallis, OR 97331-4003, U.S.A.

The crystal chemistry copper oxide superconductors is reviewed with respect to defects, stability and the n-type phases. It is concluded that the n-type copper oxide superconductors are genuine examples of reduced systems which any viable theory for high T_c must explain. Defects are crucial for the control of carrier concentration and presumably critical current. They also cause troublesome and pervasive inhomogeneities. Most, and possibly all, high T_c superconductors are thermodynamically unstable at room temperature and below.

1. INTRODUCTION

I have recently reviewed the crystal chemistry of oxide superconductors¹⁻³; thus, this paper will not be yet another overview of the crystal chemistry of these materials. Instead, I focus on the crystal chemistry issues relating to defects, stability and the n-type copper oxides. The role of defects is critical because they control carrier concentration, inhomogeneities and presumably flux pinning. The apparent lack of thermodynamic stability for high T_c superconductors is a crucial factor in the synthesis of these materials and must also be considered for any theory of the mechanism for high T_c .

2. n-TYPE COPPER OXIDES

From the point of view of our understanding of copper oxide based superconductors, the n-type copper oxides found by Tokura *et al.*⁴ represent the most significant new superconductors since the discovery of Bednorz and Müller. Different mechanisms for n- and p-type materials is a remote possibility. Thus, an important part of the correct theory must be that p- and n-type doping give essentially the same effect. This then eliminates from consideration those theories dependent on some special feature of an "oxygen 2p band", especially a π^* oxygen 2p band.

Evidence for the n-type character of certain copper oxides does not come merely from electrical transport data. There is also overwhelming evidence from the chemistry side. Several papers presented at this conference⁵⁻⁸ have amply demonstrated that these materials are now as well characterized as are most of the p-type copper oxides.

The materials first discovered to be n-type copper oxides are the $R_{2-x}Ce_xCuO_{4+y}$ series where R may be Pr, Nd, Sm, Eu or Gd.⁴ Initially, some doubts were expressed about the description of these phases because cerium is well known in

both the tetravalent and trivalent oxidation states. This issue was clouded by widespread confusion concerning the meaning of oxidation states, exemplified by the absurd notion the cerium might not be tetravalent in CeO_2 . Spectroscopic studies have now shown that cerium is tetravalent in the $R_{2-x}Ce_xCuO_4$ superconductors. Actually, the oxidation state of Ce was already clear from examination of the unit cell dimensions of the $R_{2-x}Ce_xCuO_4$ phases. We know that Ce^{IV} is smaller than the R^{III} cations and that Ce^{III} is larger than the R^{III} cations being used. Thus, we expect to see the c axis increase if cerium were trivalent. In fact, the c axis decreases with cerium substitution showing that the cerium is tetravalent. The a axis slightly increases with Ce substitution despite the smaller size of Ce^{IV} . This occurs because the a axis dimension is dominated by the Cu-O distance of the highly covalent Cu-O bond. The highest filled levels in a Cu^{II} oxide are strongly antibonding. Thus, removing electrons causes a decrease in the Cu-O bond length. Adding electrons results in an increase of the bond distance and thus an increase in the a cell dimension.

In the $R_{2-x}Th_xCuO_4$ and $Nd_2CuO_{4-x}F_x$ phases,⁶ there are no oxidation state issues for the dopants. The remaining issue is the question of precise oxygen content. Tarascon presented very careful studies at this conference⁵ showing that superconducting properties were optimized when both oxygen interstitials and vacancies were minimized. Thus from a chemistry point of view, these materials are clearly reduced, n-type systems. This is confirmed by chemical titrations for oxidation states. Various spectroscopic studies have also confirmed the reduced nature of copper in these systems.

Hall and Seebeck measurements have shown dominantly n-type behavior for these materials.

This has been true for both ceramic and single crystal materials, regardless of whether the measurement is taken parallel or perpendicular *c* axis. There are conditions for which positive Hall coefficients have been found for the $R_{2-x}Ce_xCuO_4$ phases, but there are also cases where negative Hall coefficients are found for $YBa_2Cu_3O_{8+x}$ phases.

The coordination of Cu^I to oxygen is normally two-fold linear. Thus, Cu^I in the square planar coordination of the *T* structure might seem implausible. However, there are examples where the coordination of Cu^I to oxygen is four fold and not tetrahedral.⁹ More importantly, examination of the causes of two-fold linear coordination for Cu^I leads one to believe that square planar coordination for Cu^I is more favorable in oxides than is tetrahedral coordination. Frequently, the bonding of Cu^I is simply viewed as utilizing *s* and *p* orbitals of copper because the *3d* shell is filled. However, the pervasiveness of "*sp*" bonding and lack of *sp*² and *sp*³ bonding for Cu^I in oxides cannot be understood on this basis. We must assume that the filled *3d* core interferes with *s-p* bonding. Thus, the prerequisite for bond formation is polarization of the filled core through *s-d* hybridization.¹⁰ The usual occurrence is that the core polarizes from a sphere to a disk. Thus, only two strong bonds may form along the unique axis of this disk. However, *s-d* hybridization could as well polarize the core to give an egg-shaped ellipsoid. Then, the strong Cu^I -O bonds would form perpendicular to the unique axis, and this is consistent with square planar coordination for Cu^I . This situation is analogous to the Jahn Teller effect found for *d*⁸ cations such as Cu^{III} . The usual occurrence of this Jahn Teller distortion of an octahedron is that we see four short and two long bonds. A two-short, four-long configuration is energetically equivalent to the first approximation. However, this configuration is only rarely found. Likewise, four short bonds for Cu^I is only rarely found in oxides even though its energetics are not so unfavorable in the square planar configuration.

The existence of both n- and p-type copper oxides suggests a schematic phase diagram and band structure as shown in Figure 1. The symmetry is exaggerated in both parts of this figure, but I doubt that the deviations from this ideal symmetry are important for a basic understanding of these materials. At the midpoint of the schematic phase diagram, all copper is divalent and the σ^* band is split to give an antiferromagnetic insulator. States near the Fermi level are derived nearly equally from oxygen and copper; thus, labeling bands near the Fermi level as $Cu\ 3d$ or as $O\ 2p$ is misleading.

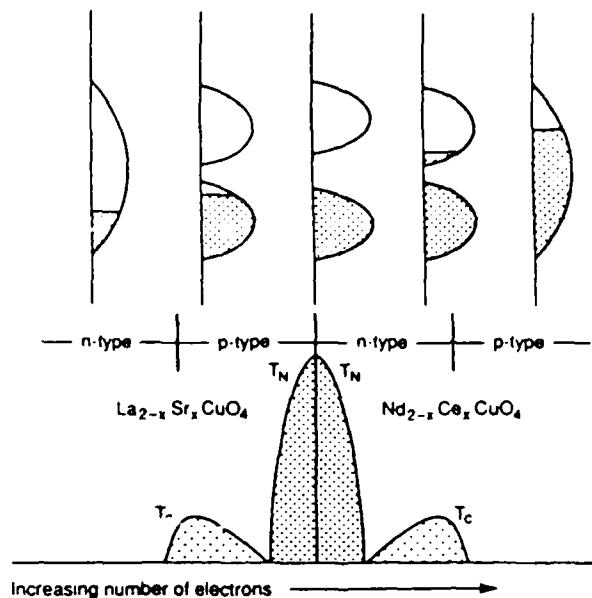


FIGURE 1
Schematic phase diagram (lower) and schematic band structures (upper) for A_2CuO_4 phases, both n- and p-types

Reduction of Cu^{II} , adding electrons from the midpoint, leads to n-type materials. Oxidation of Cu^{II} , removing of electrons from midpoint, leads to p-type materials. Doping either way destroys the antiferromagnetic state. Sufficient doping produces conductors which superconduct. The materials with the highest doping levels are incompletely characterized. They are difficult to prepare single phase, and single crystals are not yet available. Nonetheless, current evidence suggests that the carrier type switches as superconductivity disappears. This is consistent with a view that the splitting of the σ^* band disappears at high doping levels.

The π^* band, which overlaps the filled part of the σ^* band, is ignored in this figure. The observed symmetry between electron and hole carriers suggests that this π^* band can be safely ignored for a basic understanding of these materials. However, until T_c 's for n-type materials match those for p-type materials, it is natural to think that the π^* band plays some role in enhancing T_c .

The symmetry of the phase diagram (Fig. 1) has been exaggerated. Nonetheless, the optimum doping level is essentially the same for the p- and n-doping, *i.e.* about 0.15 electrons or holes per copper. This is additional evidence that reference to copper oxidation states is appropriate despite

the high covalency with strong copper-oxygen admixture in the region of the Fermi level.

There are several significant departures from the symmetry shown in the schematic phase diagram (Fig. 1). For the n-type materials, the magnetic insulating state actually disappears more slowly.¹¹ The superconducting state is observed over a more narrow range of doping, and T_c reaches only about 25 K instead of about 35 K for the p-type phases. This lack of symmetry may well be related to the fact that the σ^* states generally derive more from copper and less from oxygen as the σ^* band fills.

The scale has been purposely left off the horizontal axis of the phase diagram. This is because all doped materials are intrinsically inhomogeneous, and the scale of the horizontal axis thus becomes confused. We will come back to this inhomogeneity issue in the next section. However, this confusion in no way invalidates the general trends shown in the phase diagram section of Figure 1.

One of the most inappropriate questions ever asked of the p-type copper oxides was whether the hole was an oxygen or copper. The question was inappropriate because of the high degree of copper-oxygen admixture near the Fermi level. Also, we know that the holes would not develop reasonable mobility if they did not spend significant time on both copper and oxygen. Actually, it is best to think of the holes as being on neither copper nor oxygen. Instead, they reside in the bonds between copper and oxygen.

Once the question was asked as to whether the holes were on copper or oxygen, people rose to the challenge to provide an answer. Evidence was found for oxygen 2p character for the holes. Thus, some too quickly concluded that the holes were on oxygen alone. However, equally good evidence has been found that the holes have copper 3d character. This evidence come from XAS studies¹² as well as XPS studies of both core peaks¹³ and the valence region.¹⁴ The best current estimate of the relative contributions of oxygen and copper at the Fermi level is that the states derived about 70% from oxygen and 30% from copper.¹⁴ Taking into account the composition of the sheets, CuO_2 , the conclusion is that the individual atoms of the sheets are contributing nearly equally to states near the Fermi level.

3. DEFECTS

Defects in the copper oxide systems are both a curse and a blessing. We could not control carrier concentrations without the defects, and it is variation of carrier concentration that has given us our most interesting trends with T_c , T_N , etc. Defects are also the hope for improving the critical cur-

rent in the copper oxide based superconductors. Finally, defects cause inhomogeneities which plague us continuously.

Solid solutions, including systems of the type $\text{La}_{2-x}\text{Sr}_x\text{CuO}_4$, are intrinsically inhomogeneous. The substitution of Sr for La creates a point defect. Electronic properties in the vicinity of Sr are different than elsewhere in the La_2CuO_4 matrix. If one uses the coherence length to set the scale for the size of significant inhomogeneity, we find that there is no value of x for which the inhomogeneities can be safely ignored. Flux exclusion data indicate that the most homogeneous superconductor in the $\text{La}_{2-x}\text{Sr}_x\text{CuO}_4$ system is for x of about 0.15. However, even this composition cannot be regarded as homogeneous because a random distribution of Sr at this concentration in the La_2CuO_4 matrix would give significant Sr-free regions which are larger than twice the coherence length.

Inhomogeneities should not be mistaken for indications of phase separation. A material may be strictly single phase in the usual thermodynamic sense and yet be very inhomogeneous in an electronic sense. The basic problem is that solid solutions and doped systems are intrinsically inhomogeneous. Sometimes, the inhomogeneities are not important for the properties of interest. However, for the oxide superconductors such as those in the $\text{La}_{2-x}\text{Sr}_x\text{CuO}_4$ system, these inhomogeneities cannot be ignored with respect to either magnetic or electronic properties. One of the disturbing consequences of this fact is that some of our probes will invariably be influenced more by the low x regions and other probes will be more influenced by the high x region of our single phase solid solutions. Thus, those performing different measurements may have great difficulty reconciling their results because they are probing different regions of a heterogeneous, single-phase material.

There are also several extended defects to consider in the oxide superconductors. In the $\text{YBa}_2\text{Cu}_3\text{O}_7$ type phases, there are both 110 twinning and 90° misorientation defects. The latter is also sometimes referred to as twinning. However, the 110 twinning and the 90° misorientations are distinctly different. The former, coherent twinning, relieves lattice strain while the latter, incoherent twinning, causes lattice strain. There has been much speculation about the roles of these two extended defects in $\text{YBa}_2\text{Cu}_3\text{O}_7$ phases. Another common extended defect is stacking faults or intergrowth. These are particularly common in the $\text{Tl,Bi/Ba,Sr/Ca,Cu/O}$ superconductors.

A new extended defect has recently been discovered by Gai¹⁵ in the La_2CuO_4 structure. This defect is essentially absent in La_2CuO_4 itself.

However in the $\text{La}_{2-x}\text{Sr}_x\text{CuO}_4$ system, this defect increases with x , at least up to $x = 0.15$. The defect may be described as a shear, and oxygen is eliminated at this defect. Thus, this system is more properly regarded as $\text{La}_{2-x}\text{Sr}_x\text{CuO}_{4-y}$ where the extended defect and y tend to increase with increasing x . Thus, the carrier concentration in these phases is expected to be somewhat less than that predicted by the value of x alone. However, this effect could be balanced off to some extent by interstitial oxygen.

It has been mysterious why T_c drops when rare earths such as Nd substituted for La in superconductors of the type $\text{La}_{2-x}\text{Sr}_x\text{CuO}_4$. Appreciable composition ranges of the type $\text{La}_{2-x-y}\text{Sr}_x\text{R}_y\text{CuO}_4$ may be prepared where R is Pr, Nd, Sm, Eu or Gd.¹⁶ The Cu-O distance in the CuO_2 sheets decreases as R becomes smaller and as y becomes larger. Nonetheless, the tendency is for T_c to drop with this substitution, the opposite of the usual correlation between T_c and Cu-O distance. We decided that a missing piece of this puzzle was the chemical analysis for the oxidation state of copper. On performing this analysis on many samples of the type $\text{La}_{2-x-y}\text{Sr}_x\text{R}_y\text{CuO}_4$, we found that for fixed x the Cu^{III} content tends to decrease as y increases and as R becomes smaller.¹⁷ In fact, these materials have the very familiar trend of T_c with Cu^{III} concentration. This strong correlation obscures the possible correlation of T_c with Cu-O distance. The shear type defects found by Gai in $\text{La}_{2-x}\text{Sr}_x\text{CuO}_4$ are also pronounced in $\text{La}_{2-x-y}\text{Sr}_x\text{R}_y\text{CuO}_4$ phases.¹⁷ We may speculate that these defects are now more numerous and that this has resulted in a greater oxygen deficiency.

Not all oxide superconductors depend on defects for all the important Cu^{III} or Cu^{I} content. The ideal formulae for $\text{YBa}_2\text{Cu}_3\text{O}_7$, $\text{YBa}_2\text{Cu}_4\text{O}_8$ and $\text{Y}_2\text{Ba}_4\text{Cu}_7\text{O}_{15}$ are all apparently appropriate to give high T_c superconductors. These then are the materials of choice if one wishes to study homogeneous materials. However, these materials are prone to have defects such as twins, misorientations and intergrowths. Therefore, their defect concentration may be significant. Another problem with all of these phases is that much of the copper is not in the CuO_2 sheets. This is not true of the other copper oxide based superconductors where the carrier concentration is controlled through the point defect concentration.

Band structure calculations had suggested that the carrier concentration in $\text{Bi}_2\text{Sr}_2\text{Ca}_{n-1}\text{Cu}_n\text{O}_{4+2n}$ phases is controlled by overlap of the Bi 6s band with the Fermi level. However, this conclusion is very much at odds with reasonable chemistry¹ and apparently resulted from the

highly idealized structure used for the calculations. The carrier concentration in these phases is instead due to deviations from the ideal stoichiometry, i.e. point defects.²

4. STABILITY

There is good reason to believe that most (or all) of the high T_c superconductors are not thermodynamically stable at room temperature and below. This is not necessarily a concern in practical terms. After all, diamond and window glass are also metastable under ambient conditions. However, optimum synthesis approaches to metastable materials are very different than those employed for thermodynamically stable phases. Also, it would seem that a viable theory must suggest an unstable lattice in a high temperature superconductor. This was, of course, relatively straightforward using classical BCS theory.

The standard synthesis of $\text{YBa}_2\text{Cu}_3\text{O}_{6+x}$ phases starts under conditions where x in the product is so small ($x \sim 0.3$) that superconducting materials are not obtained. These phases must be oxidized to obtain a high T_c superconductor. The oxidation of $\text{YBa}_2\text{Cu}_3\text{O}_6$ to $\text{YBa}_2\text{Cu}_3\text{O}_7$ is an intercalation reaction. Products made by intercalation reactions are nearly always metastable. Thus, they cannot generally be made in a direct, one-step process. All attempts to prepare $\text{YBa}_2\text{Cu}_3\text{O}_7$ in a one step process have failed. Serious attempts to obtain true equilibrium for $\text{YBa}_2\text{Cu}_3\text{O}_{6+x}$ phases indicated that the highest value of x for a thermodynamically stable phase is about 0.7.¹⁸ However, even this phase is most likely not stable at room temperature and below. After all, the most stable phase in the $\text{YBa}_2\text{Cu}_3\text{O}_{6+x}$ series ($x = 0.0$) is apparently not stable below about 500°C.

The structures of $\text{YBa}_2\text{Cu}_4\text{O}_8$ and $\text{Y}_2\text{Ba}_4\text{Cu}_7\text{O}_{15}$ are, of course, very closely related to that of $\text{YBa}_2\text{Cu}_3\text{O}_7$, and it would appear that both $\text{YBa}_2\text{Cu}_4\text{O}_8$ and $\text{Y}_2\text{Ba}_4\text{Cu}_7\text{O}_{15}$ are thermodynamically stable phases under the conditions where they are prepared. There is no current evidence that these materials become unstable at lower temperature, very unlike the next compounds to be considered.

Our highest T_c 's have been found for compounds which are ideally represented as $(\text{A}'\text{O})_x\text{A}_2\text{Ca}_{n-1}\text{Cu}_n\text{O}_{2n+2}$ where A' is Tl or Bi and A is Ba or Sr. Actually, these phases are always ridden with defects resulting in substantial deviations from this ideal formulation. These phases have only been prepared at high temperatures, very close to melting temperatures. All low temperature synthesis routes have failed. Also, exotherms of compound formation have never been noted for these compounds when they are prepared from the binary oxides. Thus, there is good reason to believe that these phases are

endothermic compounds, i.e., they are stabilized by entropy and are not stable at lower temperatures.

Entropy stabilized oxide compounds are rare but known. Well studied examples are CuFe_2O_4 , Fe_2TiO_3 and $\text{Al}_6\text{Si}_2\text{O}_{13}$.¹⁹ In all of these cases, the disorder giving the entropy for compound stabilization is in the form of point defects.

Thus, the $(\text{A}'\text{O})_x\text{A}_2\text{Ca}_{n-1}\text{Cu}_n\text{O}_{2n+2}$ superconductors appear to cases of entropy stabilized phases, i.e., they are stable under their synthesis conditions but not at lower temperatures. They are defect ridden, and apparently these defects are required for the stabilization of these phases. This also means that these phases will tend to be inhomogeneous even though we frequently represent them with ideal formulae.

Solid solutions or doped systems are trivial examples of entropy stabilized systems. Thus, superconductors such as $\text{La}_{2-x}\text{Sr}_x\text{CuO}_4$ and $\text{Nd}_{2-x}\text{Ce}_x\text{CuO}_4$ are not expected to be thermodynamically stable at low temperatures. In fact, the thermodynamic stability range appears to be sufficiently restricted to preclude low temperature synthesis of these phases.

5. CONCLUSIONS

The chemistry case for the n-type copper oxides is overwhelming. These materials are what they appear to be, and successful theory must account for this symmetry at the Fermi level.

Defects control many of the properties of interest. We are still struggling to control and measure defect concentration. Much work remains to relate defects to flux pinning. The defects lead inescapably to inhomogeneities in most of the oxide superconductors. We cannot afford to ignore these inhomogeneous materials which make up the bulk of the high temperature superconductors. Instead, we must learn to model this inhomogeneity.

Most oxide superconductors are thermodynamically unstable. It remains to be shown whether or not they are all metastable. For those we now know to be metastable, rational synthesis techniques must take into account this lack of thermodynamic stability.

ACKNOWLEDGEMENT

Some support for the presentation of this work was provided by the Department of Navy Grant N00014-80-J-1000 and the Office of Naval Research. The United States Government has a royalty-free right throughout the world in all copyrightable material contained herein.

REFERENCES

1. A.W. Sleight, *Science* **242** (1988) 1519.
2. A.W. Sleight, M.A. Subramanian and C.C. Torardi, *Mater. Res. Soc. Bull.* **14** (1989) 45.
3. A.W. Sleight in *High Temperature Superconducting Materials*, Edited by Hatfield and Miller (Dekker, NY, 1988), p1.
4. Y. Tokura, H. Takagi and S. Uchida, *Nature* **337** (1989) 345.
5. J.M. Tarascon, these proceedings.
6. B. Maple, these proceedings.
7. S. Uchida, these proceedings.
8. Z. Fisk, these proceedings.
9. E.M. McCarron and J. Calabrese, *J. Solid State Chem.* **62** (1986) 64 and **65** (1986) 215.
10. A.W. Sleight, Proceedings of the XXXII Welch Conference, 1988.
11. Y.J. Uemura, these proceedings.
12. E.E. Alp, G.L. Goodman, L.Soderholm, S.M. Mini, M. Ramanathan and G.K. Shenoy, *J. Phys. Chem.*, in press.
13. A. Balzarotti, et al., *Phys. Rev.* **B38** (1988) 646 and W.R. Flavell and R.G. Egdell, *Phys. Rev.* **B39** (1989) 231.
14. A.J. Arko, these proceedings.
15. P. Gai, in press.
16. for example, J.M. Tarascon, L.H. Greene, W.R. McKinnon and G.W. Hull, *Solid State Commun.* **63** (1987) 499.
17. M.A. Subramanian, P. Gai, J. Gopalkrishna and A.W. Sleight, in press.
18. J. Karpinski, E. Kaldis, E. Jilek and S. Rusiecki, *Nature* **336** (1988) 660 and D.E. Morris et al. *Phys. Rev.* **B39** (1989) 7347.
19. A. Navrotsky, in *Solid State Chemistry*, Edited by Cheetham and Day (Clarendon Press, Oxford, 1987), p382.

REPORT DOCUMENTATION PAGE

1a. REPORT SECURITY CLASSIFICATION UNCLASSIFIED			1b. RESTRICTIVE MARKINGS		
2a. SECURITY CLASSIFICATION AUTHORITY			3. DISTRIBUTION/AVAILABILITY OF REPORT		
2b. DECLASSIFICATION/DOWNGRADING SCHEDULE					
4. PERFORMING ORGANIZATION REPORT NUMBER(S)			5. MONITORING ORGANIZATION REPORT NUMBER(S)		
6a. NAME OF PERFORMING ORGANIZATION Department of Applied Physics		6b. OFFICE SYMBOL (If applicable)	7a. NAME OF MONITORING ORGANIZATION Office of Naval Research		
6c. ADDRESS (City, State and ZIP Code) Stanford University Stanford, California 94305			7b. ADDRESS (City, State and ZIP Code) 800 North Quicy Street Arlington, Virginia 22217-5000		
8a. NAME OF FUNDING/SPONSORING ORGANIZATION		8b. OFFICE SYMBOL (If applicable)	9. PROCUREMENT INSTRUMENT IDENTIFICATION NUMBER		
8c. ADDRESS (City, State and ZIP Code)			10. SOURCE OF FUNDING NOS.		
			PROGRAM ELEMENT NO.	PROJECT NO.	TASK NO.
			WORK UNIT NO.		
11. TITLE (Include Security Classification) International Conference on Materials and Mechanisms of Superconductivity: High Temperature Superconductors					
12. PERSONAL AUTHOR(S) Professor T.H. Geballe (PI)					
13a. TYPE OF REPORT Final Technical		13b. TIME COVERED FROM 3/15/89 TO 3/14/90	14. DATE OF REPORT (Yr., Mo., Day) 1989 October 30		15. PAGE COUNT 32
16. SUPPLEMENTARY NOTATION					
17. COSATI CODES			18. SUBJECT TERMS (Continue on reverse if necessary and identify by block number)		
FIELD	GROUP	SUB. GR.			
19. ABSTRACT (Continue on reverse if necessary and identify by block number)					
<p>The proceedings included herewith represent the contributions of ONR speakers at the International Meeting on the Materials and Mechanisms of Superconductivity -- High-Tc held at Stanford on July 23-28, 1989. The following speakers and topics are included: J.R. Clem, 'Phenomenological Theory of Magnetic Structure in the High-Temperature Superconductors'; V. Kogan, 'Anisotropy in Magnetic Properties of High-Tc Materials'; D.R. Nelson, 'Melted Flux Liquids in High-Tc Superconductors'; C.G. Olson, 'High Resolution-Angle Resolved Photoemission Studies of High Temperature Superconductors'; S.C. Zhang, 'Spin Fluctuations, Spin Bags and the High Tc Superconductivity'; A.W. Sleight, 'Crystal Chemistry of Oxide Superconductors'; Y.J. Uemura, 'Probing Magnetism and Superconductivity of High-Tc Systems with Positive Muons'. In addition partial ONR support was given to J. Hirsch and R. Joynt. Those attendees have decided to publish their results elsewhere, and therefore they are not included in the present proceedings.</p>					
20. DISTRIBUTION/AVAILABILITY OF ABSTRACT UNCLASSIFIED/UNLIMITED <input checked="" type="checkbox"/> SAME AS RPT. <input type="checkbox"/> DTIC USERS <input type="checkbox"/>			21. ABSTRACT SECURITY CLASSIFICATION		
22a. NAME OF RESPONSIBLE INDIVIDUAL T.H. Geballe		22b. TELEPHONE NUMBER (Include Area Code) (415) 723-0215		22c. OFFICE SYMBOL	